

# 000 INFERRING THE INVISIBLE: NEURO-SYMBOLIC RULE 001 DISCOVERY FOR MISSING VALUE IMPUTATION 002

003 **Anonymous authors**  
004

005 Paper under double-blind review  
006

## 007 ABSTRACT 008

009 One of the central challenges in artificial intelligence is reasoning under partial  
010 observability, where key values are missing but essential for understanding and  
011 modeling the system. This paper presents a neuro-symbolic framework for latent  
012 rule discovery and missing value imputation. In contrast to traditional latent variable  
013 models, our approach treats missing grounded values as latent predicates to be  
014 inferred through logical reasoning. By interleaving neural representation learning  
015 with symbolic rule induction, the model iteratively discovers—both conjunctive  
016 and disjunctive rules—that explain observed patterns and recover missing entries.  
017 Our framework seamlessly handles heterogeneous data, reasoning over both dis-  
018 crete and continuous features by learning soft predicates from continuous values.  
019 Crucially, the inferred values not only fill in gaps in the data but also serve as  
020 supporting evidence for further rule induction and inference—creating a feedback  
021 loop in which imputation and rule mining reinforce one another. Using coordinate  
022 gradient descent, the system learns these rules end-to-end, enabling interpretable  
023 reasoning over incomplete data. Experiments on both synthetic and real-world  
024 datasets demonstrate that our method effectively imputes missing values while  
025 uncovering meaningful, human-interpretable rules that govern system dynamics.  
026

## 027 1 INTRODUCTION 028

029 Neural-symbolic reasoning combines the pattern recognition power of neural networks with the  
030 precision and interpretability of symbolic reasoning (Hitzler & Sarker, 2022; Yang et al., 2024).  
031 This hybrid paradigm enables AI systems to detect complex patterns in unstructured data while  
032 reasoning about them in a structured and explainable manner.

033 Traditional rule induction methods extract explicit patterns from observed data but often fail when  
034 *some observations are missing or incomplete* (Campero et al., 2018; Claire Glanois, 2022). These  
035 approaches can effectively learn surface-level rules, yet their ability to fully explain the underlying  
036 system is limited when essential data points are absent. For example, in healthcare diagnostics,  
037 critical measurements may be missing or noisy, making accurate imputation necessary for reliable  
038 reasoning.

039 Probabilistic models such as Markov Logic Networks (MLNs) (Richardson & Domingos, 2006)  
040 handle missing data by treating unobserved facts as latent predicates. However, they typically rely  
041 on a *fixed rule base* and *expensive joint inference*, limiting scalability and adaptability in large or  
042 heterogeneous datasets (Oltramari et al., 2020). In contrast, we propose a neuro-symbolic system  
043 that *co-learns rules and imputations* in a single differentiable loop, enabling fast forward-chaining  
044 inference and end-to-end learning.

045 Our core idea is *a closed loop between imputation and rule discovery*. Given partially observed  
046 tables with discrete and continuous attributes, we treat each missing, entity-specific entry as an un-  
047 known fact and apply learned rules in a *forward-chaining* pass to predict it. These predictions are  
048 compared to the observed entries via a supervised loss, and backpropagation updates the rule param-  
049 eters and soft predicates. Crucially, improved imputations provide additional evidence for discover-  
050 ing and refining rules in subsequent passes. This self-reinforcing loop leads to better imputations,  
improved rule induction, and stronger downstream inference.

051 To enable multi-hop reasoning at scale, many targets require compositional explanations in the form  
052 of chains and disjunctions. We optimize rule embeddings using *asynchronous coordinate gradient*  
053 *descent*, updating one rule or clause at a time while holding others fixed. This mirrors step-wise  
reasoning and ensures monotone loss progress on a smooth surrogate. For disjunctive heads, we

054 adopt a sequential covering strategy to harvest diverse clauses, followed by joint fine-tuning using a  
 055 soft-OR aggregator (LogSumExp) to reconcile interactions. This staged procedure reliably recovers  
 056 long chains and disjunctive theories under high missingness while keeping computation tractable.  
 057

058 Our framework handles heterogeneous data by learning *soft predicates* for continuous features (us-  
 059 ing sigmoid thresholds and slopes) and combining them with discrete predicates through differen-  
 060 tiable logical operators. Specifically, we use soft-min to approximate logical AND and soft-max  
 061 to approximate logical OR. This approach enables uniform forward chaining over mixed data types  
 062 without requiring pre-discretization.

063 **Contributions.** We summarize our contributions as follows: (i) We introduce a closed-loop neuro-  
 064 symbolic framework in which imputation and rule discovery mutually reinforce each other, rather  
 065 than treating imputation as a preprocessing step. (ii) We develop a scalable coordinate gradient  
 066 descent scheme, combined with sequential covering and joint fine-tuning, that enables multi-hop  
 067 and disjunctive rule learning even under high missingness. (iii) We design a unified differentiable  
 068 forward-chaining engine that handles both discrete and continuous attributes through soft predicates  
 069 and smooth logical operators. (iv) We empirically validate our approach on synthetic chain and dis-  
 070 junction tasks, as well as real-world datasets (Birds, Heart, SPECT), demonstrating that it recovers  
 071 human-interpretable rules while achieving strong imputation accuracy and downstream prediction  
 072 performance.

## 073 2 RELATED WORK

074 Our work is at the intersection of neuro-symbolic Inductive Logic Programming (ILP) and missing  
 075 value imputation.

076 **Neural Embedding-based ILP.** Embedding-based models are widely used for Knowledge Base  
 077 (KB) completion like TransE (Bordes et al., 2013), TransH (Wang et al., 2014), and TransR (Lin  
 078 et al., 2015). Complex (Trouillon et al., 2016) introduces complex-valued embeddings for asym-  
 079 metric relations, while multi-hop reasoning methods like Guu et al. (2015) leverage path-based  
 080 embeddings for traversing knowledge graphs. However, these approaches often face limitations in  
 081 reasoning power.

082 Recent advances in ILP integrate symbolic logic with neural networks. Rocktäschel & Riedel (2017)  
 083 propose *Neural Theorem Proving (NTP)*, which uses a differentiable backward-chaining method.  
 084 Then, Campero et al. (2018) introduces a neural forward-chaining differentiable rule induction  
 085 network. However, both rely on hand-designed templates. Claire Glanois (2022) advances these models  
 086 by incorporating a hierarchical structure, enabling more flexible rule induction. Nevertheless, these  
 087 methods are primarily designed for fully-observed data and struggle to handle missing values.

088 **Interpretable Rule Learning.** Learning interpretable logical rules for classification has been a  
 089 long-standing goal. Dash et al. (2018) propose **BRCG**, an integer programming approach that uses  
 090 column generation to efficiently search the exponential space of candidate clauses, explicitly balanc-  
 091 ing classification accuracy with rule simplicity. Wang et al. (2021) introduce **RRL**, which utilizes  
 092 a Gradient Grafting mechanism to learn non-fuzzy rule lists within a deep learning framework,  
 093 ensuring scalability. Qiao et al. (2021) propose **DR-NET** to learn independent decision rules in  
 094 Disjunctive Normal Form (DNF) by jointly optimizing rule generation and weight learning. More  
 095 recently, Barbiero et al. (2022) present **LEN**, an end-to-end differentiable neuro-symbolic method  
 096 that leverages an entropy-based criterion to extract concise First-Order Logic explanations from  
 097 neural networks. Unlike these methods, which focus primarily on classification tasks with complete data  
 098 with binary features, our framework integrates rule learning directly with the handling of missing  
 099 values.

100 **Rule-Based Missing Value Imputation.** Traditional missing data imputation methods, ranging  
 101 from statistical techniques like **MICE** (Multivariate Imputation by Chained-Equations) (van Bu-  
 102 ren & Groothuis-Oudshoorn, 2011), **MissForest** (Random Forest based) (Stekhoven & Bühlmann,  
 103 2012), and SOFT-IMPUTE (Mazumder et al., 2010) to deep learning models like **GAIN** (GAN-  
 104 based) (Yoon et al., 2018), **MissDiff** (Diffusion-based)(Ouyang et al., 2023), **mDAE** (DAE-  
 105 based)(Dupuy et al., 2024), **VAE-based**(Veldkamp et al., 2025) and MMDL (Li et al., 2020), typ-  
 106 ically rely on statistical patterns and do not leverage explicit logical rules to govern inter-variable  
 107 relationships (see Appendix A for a detailed overview).

108 Recent works have started to bridge rule-based reasoning and missing value imputation. For in-  
 109 stance, Chen et al. (2023) employ various interpretable machine learning techniques to address the  
 110 missing value problem, but their methods are not explicitly rule-based. Closer to our approach,

108 MINTY (Stempfle & Johansson, 2024) utilizes a rule-based model to handle missing data; however,  
 109 it does not leverage neuro-symbolic reasoning to learn the intricate relationships between observed  
 110 and missing values as we do. Other non-neural approaches, such as the work by Wang et al. (2017)  
 111 on synthesizing data completion, also tackle the problem but lack of the representation learning  
 112 capabilities of neural networks. Our work is distinct in its tight integration of neural learning for  
 113 representation and symbolic reasoning for both rule discovery and imputation, forming a feedback  
 114 loop where each component enhances the other.

### 3 BACKGROUND

117 **Predicate.** In the context of logic-based AI systems, a predicate is a fundamental Boolean logic  
 118 variable used to describe properties of or relationships between entities. Predicate variables are  
 119 grounded by data, being True or False, and serve as the basic building blocks for logical expressions.  
 120 For instance, a predicate like *Has\_Fever(Patient)* denotes whether a patient has a fever, while  
 121 *Use\_Drug(Patient)* specifies whether a drug treats a particular patient. These predicates capture  
 122 essential aspects of the system’s state and relationships.

123 **Logic Rules and Forward Chaining.** We represent knowledge with **Horn clauses**

$$f : Q \leftarrow P_1 \wedge P_2 \wedge \dots \wedge P_h, \quad (1)$$

124 where  $P_1, \dots, P_h$  (the *body*) are conditions and  $Q$  (the *head*) is the conclusion. Given observed  
 125 facts (the evidence set  $\mathcal{E}$ ), we perform *forward chaining*: whenever all body predicates of a rule  
 126 are (approximately) satisfied by facts in  $\mathcal{E}$ , the rule *fires* and adds  $Q$  to  $\mathcal{E}$ . Importantly, newly  
 127 inferred facts are *immediately recycled as evidence*, enabling *multi-hop reasoning*—cascades of rule  
 128 applications that derive conclusions not reachable in a single step.

129 **Latent Predicates and Rule Learning.** We use the term *latent predicate* to denote an unobserved  
 130 fact tied to concrete entities (and, when relevant, timestamps) within the same relational schema as  
 131 observed predicates. Latent predicates may be Boolean or soft-valued (degrees of truth); they repre-  
 132 sent missing-but-specific facts we wish to infer. Our goal is to learn *Horn rules* of the form Eq. (1)  
 133 that capture regularities among observed predicates and support inference about latent ones—i.e.,  
 134 rules whose heads or intermediate conclusions may involve latent predicates, enabling principled  
 135 completion of missing facts.

136 **Expressive Rule Forms.** We consider rules that capture rich logical structure, including conjunc-  
 137 tions (AND), disjunctions (OR via multiple clauses), and *chained dependencies*. For example, a  
 138 latent predicate  $Q_k$  may be characterized by

$$Q_k = (P_1 \wedge P_2) \vee (P_3 \wedge P_4),$$

139 or by multi-hop compositions such as

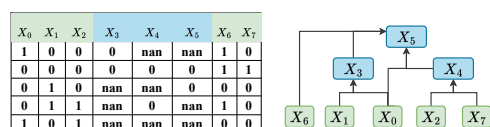
$$Q_1 = P_1 \wedge P_2, \quad Q_2 = P_3 \wedge P_4, \quad Q_3 = (Q_1 \wedge P_5) \vee (Q_2 \wedge P_6).$$

140 This view accommodates both single-step and multi-step (multi-hop) reasoning patterns within a  
 141 unified Horn-rule framework. We also allow *predicate invention*: introducing unlabeled latent pre-  
 142 dictates that are not predefined in the schema but are useful intermediates for explaining the data.  
 143 These invented predicates participate in rules just like observed ones. After rules are discovered,  
 144 their roles can be *post-hoc interpreted* by inspecting the clauses in which they appear and their  
 145 relationships to observed predicates.

### 4 MODEL: NEURO-SYMBOLIC FORWARD CHAINING NETWORK

146 Consider problems where some information or  
 147 features are incomplete. Our goal is to learn a  
 148 set of logical rules that explain how each predi-  
 149 cate with information can be imputed based on  
 150 evidence from feature space  $\mathbf{X}$ .

151 These missing variables are inferred through a  
 152 rule-learning process, allowing the model to un-  
 153 cover hidden relationships in the data. For clar-  
 154 ity, we identify the predicates with missing in-  
 155 formation as  $\mathbf{U}$ , also named as “latent predi-  
 156 cate” in our setting. Though in our experiments, we do not strictly distinguish between feature  
 157 predicates, as any of them can be incomplete and serve as latent predicates. In more general settings  
 158 with a predictive label  $Y$ , we can view  $Y$  as one of the latent predicates, making the rule learning  
 159 and prediction for  $Y$  equivalent to inferring latent predicates  $\mathbf{U}$  with rules.



153 Figure 1: Example of missing variables imputation  
 154 with rule discovery.  $X_i$  with *nan* is the pre-  
 155 dictates with missing information, which can be in-  
 156 ferred by the logic rules from  $\mathbf{X}$ .

To summarize, our model learns logical rules to infer latent predicates  $\mathbf{U}$  by discovering hidden structures within data, as an example illustrated in Figure 1. This rule induction process identifies logical relationships among observable predicates  $\mathbf{X}$  and other inferred latent predicates. By explicitly learning these structures, our approach enhances both inference capability and interpretability, offering clear insights into complex, otherwise hidden dependencies. The key idea is summarized in Figure 2, with details presented in the following sections.

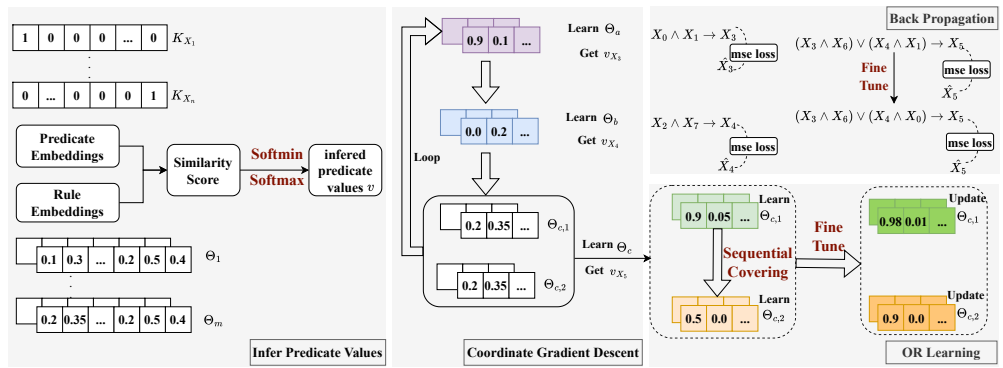


Figure 2: Model framework. Rule embeddings  $\Theta$  are optimized using coordinate gradient descent. In each learning step, predicate values are inferred via the Softmin-Softmax operation (Eqs. (3, 4,5)). For disjunctive (OR) rule learning, sequential hard covering is applied, followed by fine-tuning of the learned rule embeddings (Section 5.2). Errors are back-propagated using MSE loss between inferred predicate values and the small portion of observed latent predicate samples, constituting a weak-supervision setting.

#### 4.1 MODEL PREPARATION: PRETRAINED PREDICATE EMBEDDINGS

We begin by defining two sets of predicates:  $\mathbf{X} = \{X_1, \dots, X_n\}$  represents the set of *observable* predicate variables, and  $\mathbf{U} = \{U_1, \dots, U_m\}$  denotes the set of predicate variables with *missing information* that the model aims to discover and define. Our framework is designed to handle **both binary (categorical) and continuous features within a unified logical structure**. Binary features are treated as standard logical predicates. For continuous features, we introduce a mechanism to derive a “soft” truth value, effectively creating learnable predicates from them. This allows the model to reason over heterogeneous data types, as detailed in Section 4.2.

As mentioned before, we do not distinguish  $\mathbf{X}$  and  $\mathbf{U}$  in the experiment, as any predicates can be the predicate with missing information. We just use separate notations for model description. We initialize a fixed, unique embedding for each predicate, whether observable or missing. For example, these embeddings can be instantiated as one-hot vectors within an embedding space of dimension  $d$ . We denote the collection of embeddings for observable predicates as  $\mathbf{K}_X$  and incomplete predicates as  $\mathbf{K}_U$ . These predicate embeddings remain frozen throughout the rule learning phase and serve as a foundational dictionary, enabling the interpretation of the composition of learned rules by relating rule components back to specific predicates.

With the predicate representations defined, we next describe the core of our model: the representation of logical rules and the mechanism by which inferences are drawn.

#### 4.2 MODEL BACKBONE: RULE REPRESENTATION AND INFERENCE

In our NS-FCN framework, logical rules are materialized as learnable rule embeddings, which are the primary trainable parameters. Our model employs an asynchronous coordinate descent learning process. This learning scheme is particularly well-suited for discovering complex logical structures such as chained dependencies (where one latent predicate forms part of the definition of another) and disjunctive rules (where a latent predicate can be satisfied by one of several distinct conditions).

##### 4.2.1 SPECIFICATION OF RULE EMBEDDINGS $\Theta$

Let  $\mathcal{F}$  be the set of rules/clauses, and let  $\Theta = \{\Theta_f\}_{f \in \mathcal{F}}$  be their embeddings. Each  $\Theta_f$  encodes one rule with head predicate  $U_j$ , and a single head predicate  $U_j$  may be associated with multiple rules (OR-of-ANDs).

*Conjunctive Rule Embedding.* For a latent predicate  $U_j$  that is defined by a single conjunctive rule (e.g.,  $U_j = X_a \wedge X_b$ ), its corresponding rule embedding  $\Theta_f = [\theta_1, \dots, \theta_h] \in \mathbb{R}^{d \times h}$ . Here,  $h$  represents the number of predicates forming the body of the conjunctive rule (the arity of the conjunction, e.g.,  $h = 2$  for  $X_a \wedge X_b$ ), and  $d$  is the dimensionality of the predicate embeddings. Each of the  $h$  rows in this matrix is learned to align with the embedding of one of the constituent predicates in the rule’s body.

*Disjunctive Rule Embeddings.* If a latent predicate  $U_k$  is defined by a disjunction of  $R_k$  distinct conjunctive clauses (e.g.,  $U_k = \bigvee_{r=1}^{R_k} (\text{clause}_r)$ ), it will be associated with a set of  $R_k$  distinct rule embeddings, denoted  $\{\Theta_{k,1}, \dots, \Theta_{k,R_k}\}$ . Each individual rule embedding  $\Theta_{k,r}$  is itself an  $h_r \times d$  matrix, representing the  $r$ -th conjunctive clause, where  $h_r$  is the arity of that specific clause.

All rule embeddings are initialized randomly prior to training and are subsequently optimized as described in Section 5. Given these rule embeddings, the model infers the truth values (or continuous approximations thereof) of latent predicates through a carefully defined inference mechanism.

**Parameters for Continuous Predicates.** For each continuous feature  $f \in \mathcal{F}_C$ , where  $\mathcal{F}_C$  is the set of continuous features, the model learns two additional scalar parameters: a threshold  $\theta_f$  and a slope  $\beta_f$ . These parameters are used to define a learnable soft predicate function that maps the continuous feature value to a probabilistic truth value, as explained next.

#### 4.2.2 INFERRING PREDICATE VALUES

The latent predicates is inferred based on the current state of observable predicates, any previously inferred latent predicate values, and the learned rule embeddings  $\Theta$ .

**Predicate Matching.** Each column  $\theta_j (j = 1, \dots, h)$  in the rule embedding  $\Theta_f$  is matched with a corresponding predicate embedding. This matching is achieved by finding the predicate embedding most similar to  $\theta_j$  using cosine similarity:

$$K_j^* = \underset{K \in \mathbf{K}}{\operatorname{argmax}} \cos(K, \theta_j), \quad j = 1, \dots, h \quad (2)$$

where  $\mathbf{K} = \mathbf{K}_X \cup \mathbf{K}_U$  represents the set of all available predicate embeddings. The inverse mapping  $I(K)$  maps a predicate embedding  $K \in \mathbb{R}^d$  back to its corresponding index. Thus, indices  $1, \dots, (n+m)$  correspond to  $n+m$  predicate embeddings.

**Predicate Truth Values.** Once the best matching predicate  $K_j^*$  is identified for a rule component  $\theta_j$ , we determine its truth value, denoted as  $t_j$ . The calculation depends on whether the corresponding feature is binary or continuous:

1) For a *binary feature* (e.g., from one-hot encoding), its truth value is its current value in the data tensor:  $t_j = v^t(I(K_j^*))$ .

2) For a *continuous feature*, its truth value is computed using a learnable **soft predicate** function (a sigmoid):  $t_j = \sigma(\beta_{f_j} \cdot (v_{f_j} - \epsilon_{f_j}))$  where  $v_{f_j}$  is the value of the feature corresponding to  $K_j^*$  (i.e.  $v_{f_j} = v^t(I(K_j^*))$ ),  $\epsilon_{f_j}$  and  $\beta_{f_j}$  are its learned parameters, and  $\sigma(\cdot)$  is the sigmoid function. This allows learning soft boundaries like “ $v_{f_j} > \epsilon_{f_j}$ ”.

**Conjunctive Clause Inference (Soft-AND).** The value for a conjunctive clause is then computed by aggregating the contributions of all its components, modeling a Soft-AND operation. The contribution of each component  $j$  is the product of its similarity score and its truth value. The aggregated value is:

$$v = \prod_{j=1, \dots, h} \cos(K_j^*, \theta_j) \cdot t_j, \quad (3)$$

where  $v^t$  is the current value for observable predicates or any previously imputed values. At the beginning,  $v^t$  is all from observable predicates. With the optimization steps of coordinate descent,  $v^t$  is updated based on the refined  $\Theta$ .

To address the potential issue of diminishing values, we can use the min function instead:  $v = \min_{j=1, \dots, h} \{\cos(K_j^*, \theta_j), t_j\}$ .

However, to make this function *differentiable*, we approximate the min function using the softmax function. For each component  $j$ , there are two terms: the similarity score  $\cos(K_j^*, \theta_j)$  and the truth value  $t_j$ . The softmax is applied to the set of all  $2h$  such terms:

$$\text{softmax}(x_1, \dots, x_{2h}; \Theta) = -\frac{1}{\tau} \log \left( \frac{1}{2h} \sum_{i=1}^{2h} e^{-x_i/\tau} \right) \quad (4)$$

where each  $x_i$  represents one of the  $2h$  terms (all similarity scores and all truth values), and  $\tau$  is

270 a temperature parameter controlling the smoothness of the approximation. As  $\tau$  approaches 0, the  
 271 softmin function approximates the behavior of the hard min function.

272 **Disjunctive Rule Inference (Soft-OR).** When a latent predicate  $U_k$  is defined by a disjunction  
 273 of multiple conjunctive clauses,  $U_k = \bigvee_{r=1}^{R_k} \text{clause}_{k,r}$ , its final inferred value  $v_{U_k}$  is determined  
 274 by aggregating the values of its individual clauses  $\{v_{\text{clause}_{k,1}}, \dots, v_{\text{clause}_{k,R_k}}\}$ . This aggregation is  
 275 performed using the LogSumExp (LSE) function, which serves as a differentiable soft-OR operator:

$$277 \quad v_{U_k} = \frac{1}{\beta} \log \sum_{r=1}^{R_k} \exp(\beta \cdot v_{\text{clause}_{k,r}}), \quad (5)$$

279 where  $\beta$  is a temperature parameter. As  $\beta \rightarrow \infty$ , the LSE function increasingly approximates  
 280 the true max operator, thereby hardening the OR logic. Conversely, smaller values of  $\beta$  yield a  
 281 softer aggregation. The model’s ability to discover meaningful rules and infer latent predicate states  
 282 accurately hinges on an effective learning procedure. We now outline the training methodology  
 283 employed to optimize the rule embeddings  $\Theta$ .

## 284 5 MODEL LEARNING

286 The core of our model learning process involves training the rule embeddings  $\Theta$  by minimizing a  
 287 loss function that quantifies the discrepancy between the inferred values of latent predicates and  
 288 their partially observed truth values. Our approach leverages a sequential and staged optimization  
 289 strategy, drawing parallels with coordinate descent and incorporating elements of rule covering,  
 290 particularly for disjunctive rules. This is typically followed by a joint fine-tuning phase for rules  
 291 involving disjunctions.

### 292 5.1 COORDINATE GRADIENT DESCENT FOR RULE OPTIMIZATION

294 We employ a **block** coordinate gradient descent approach, iteratively optimizing the embedding  $\Theta_j$   
 295 for each predicate  $U_j$  (**treated as a disjoint parameter block**) while holding the embeddings of other  
 296 predicates fixed. The order in which predicates  $U_j$  are selected for optimization is randomized in  
 297 each complete pass (cycle) through all learnable latent predicates. Such optimization progress is  
 298 similar to human thinking strategy, as we humans usually draw conclusions step by step.

299 During the optimization step for a specific predicate  $U_j$  within a cycle, the inferred value  $v_{U_j}$  is ob-  
 300 tained by Eq. 3 or Eq. 4 as mentioned in the previous Section. The Mean Squared Error (MSE) loss  
 301 is computed between the inferred value  $v_{U_j}$  and its observed value  $U_{j,\text{obs}}$ , exclusively for instances  
 302 where  $U_j$  is observed, which can be viewed as a **weak supervision** setting:

$$302 \quad \mathcal{L}_{U_j} = \text{mean}((v_{U_j} \odot \text{mask}_j - U_{j,\text{obs}} \odot \text{mask}_j)^2), \quad (6)$$

303 where  $\text{mask}_j$  is a binary vector indicating observed instances of  $U_j$  ( $\text{mask}_j = 1$  indicates the obser-  
 304 vation). The rule embedding  $\Theta_j$  is then updated using gradients from this loss while all other blocks  
 305 are kept fixed, which implements a **Gauss–Seidel block coordinate gradient method** on the smooth  
 306 objective  $\mathcal{L}(\Theta) = \sum_j \mathcal{L}_{U_j}(\Theta)$ . A brief convergence discussion is provided in Appendix B.

307 After its training epochs within a cycle, if  $\Theta_j$  meets the criteria for a “perfect rule” (i.e., the impu-  
 308 tation accuracy of missing variables is larger than 0.99 and a marginal loss drop is less than  $10^{-3}$ ),  
 309 the parameters of  $\Theta_j$  will be frozen for efficient computing in subsequent cycles.

### 311 5.2 SEQUENTIAL COVERING AND FINE-TUNING OF DISJUNCTIVE RULES

312 **Sequential Covering.** When a latent predicate  $U_k$  is hypothesized to be formed by a disjunction of  
 313 multiple clauses (e.g.,  $U_k = \text{clause}_{k,1} \vee \text{clause}_{k,2} \vee \dots \vee \text{clause}_{k,R_k}$ ), its constituent rule embeddings  
 314 ( $\Theta_{k,1}, \Theta_{k,2}, \dots, \Theta_{k,R_k}$ ) are learned in a sequential manner. This iterative procedure—training a rule  
 315 embedding for a clause and then conceptually “covering” the samples it explains—is repeated for  
 316 all  $R_k$  rule clauses intended for the disjunctive predicate  $U_k$ .

317 The process begins by training the first rule embedding,  $\Theta_{k,1}$ , to capture one set of conditions  
 318 that satisfy  $U_k$ . The inferred value  $v_{\text{clause}_{k,1}}$  is computed, and the loss  $\mathcal{L}_{\text{clause}_{k,1}}$  (as per Eq. 6) is  
 319 minimized against the partially observed  $U_{k,\text{obs}}$ .

320 The learning of multiple rule clauses for a predicate  $U_k$  proceeds sequentially. After an initial clause,  
 321  $\Theta_{k,1}$ , is trained to a point where it effectively explains a subset of positive instances for  $U_k$ , a hard  
 322 covering step is employed. Specifically, training instances are considered “well-explained” if the  
 323 output of  $\Theta_{k,1}$  (i.e.,  $v_{\text{clause}_{k,1}}$ ) for these instances exceeds a high confidence threshold (e.g., 0.99).  
 These “well-explained” instances are then removed from the active training set. The training of  $\Theta_{k,1}$

concludes at this stage, and the subsequent rule clause  $\Theta_{k,2}$  is then trained on the remaining, unexplained instances of  $U_k$ . This iterative hard covering approach encourages further clause discovery of distinct rules that satisfy  $U_k$ .

**Joint Fine-tuning of Disjunctive Rules.** After the individual rule clauses for a disjunctive predicate  $U_k$  have been initialized through the sequential training and covering strategy, a joint fine-tuning phase is employed to refine these rules collectively. In this phase, the optimizer simultaneously updates all associated rule embeddings  $\{\Theta_{k,1}, \dots, \Theta_{k,R_k}\}$  for  $U_k$ . The MSE loss is computed between the combined soft-OR output  $v_{U_k}$  (obtained using Eq. 5, which aggregates the evidence from all  $R_k$  clauses) and the observed values  $U_{k,\text{obs}}$ . Given that latent predicates are, by definition, not always directly measurable, this MSE is calculated based on the small fraction of instances where the true state of the hidden predicate  $U_k$  is actually observed in the training data, which is a weakly supervised scenario:  $\mathcal{L}_{U_k,\text{finetune}} = \text{mean}((v_{U_k} \odot \text{mask}_k - U_{k,\text{obs}} \odot \text{mask}_k)^2)$ .

The optimization details, including Adam optimizer parameters and rule embedding normalizations, are illustrated in the Appendix C.1.

## 6 EXPERIMENTS

### 6.1 SYNTHETIC DATA EXPERIMENTS

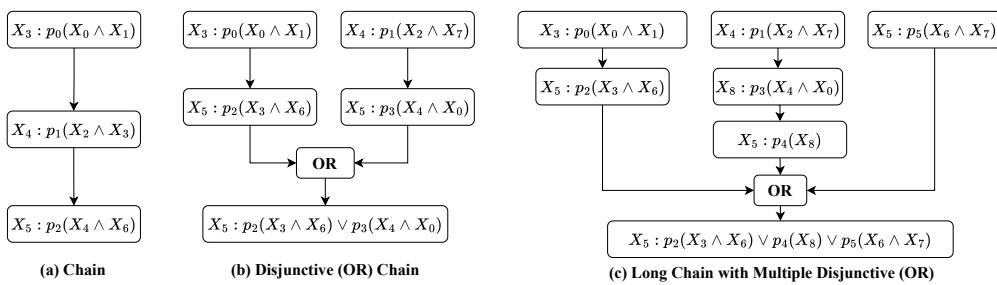


Figure 3: Example rule structures of synthetic experiments.

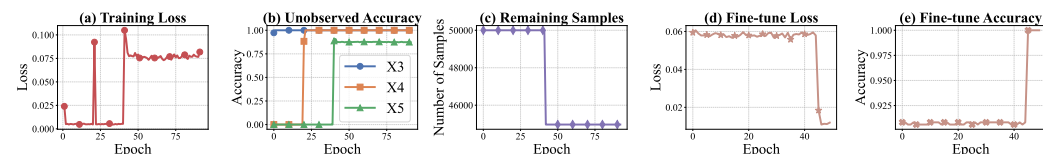


Figure 4: An example of loss and imputation accuracy during coordinate optimization (Obs. Ratio = 0.2, seed = 42). We assume the training order is  $X_3, X_4, X_5$ . Epochs 0–19 correspond to rule learning for  $X_3$ ; epochs 20–39 for  $X_4$ ; and epochs 40–end for  $X_5$ . Remaining samples identified how many samples are “well-explained” during the hard covering phase.

Table 1: Results for synthetic data example Figure 3(b) with an observation ratio of 0.2. Metrics are averaged over 20 random seeds on a dataset of 50,000 samples. Ground truth rules are underlined.

	Imp. Acc. (Before FT)	Imp. Acc. (After FT)	Train Loss (Before FT)	Train Loss (After FT)	Learned Rules	Rule Acc.
$X_3$	$1.00 \pm 0.000$	/	$0.005 \pm 0.000$	/	<u><math>X_0 \wedge X_1</math></u>	1.00
$X_4$	$0.95 \pm 0.010$	/	$0.041 \pm 0.005$	/	<u><math>X_2 \wedge X_7</math></u> , <u><math>X_0 \wedge X_7</math></u> , <u><math>X_2</math></u>	0.80
$X_5$	$0.93 \pm 0.003$	$0.96 \pm 0.002$	$0.063 \pm 0.003$	$0.067 \pm 0.001$	$(X_0 \wedge X_4) \vee (X_3 \wedge X_6)$ $(X_3 \wedge X_4) \vee (X_3 \wedge X_6)$ $(X_0 \wedge X_1) \vee (X_0 \wedge X_4)$	0.40

We use synthetic datasets to evaluate our model’s ability to learn chained and disjunctive rules under partial observability (Figure 3). Each dataset is built from observable Bernoulli variables, with missing predicates defined by ground truth rules and made partially available (10%-30% observability)

under an MCAR setting. The task is to learn rule embeddings that capture the ground truth logic, evaluated by *Rule Discovery Accuracy* (i.e. the proportion of runs which learn the truth rules) and *Imputation Accuracy*. Our method is also robust to MAR and MNAR mechanisms (Appendix E).

Table 2: Ablation Study: Effect of Fine-tuning on  $X_5$  (Disjunctive Rule) Learning

Metric for $X_5$	Before Fine-tuning	After Fine-tuning
<b>Recovered Rule Structure</b>	$(X_0 \wedge X_2) \vee (X_0 \wedge X_4)$	$(X_3 \wedge X_6) \vee (X_0 \wedge X_4)$
<b>Imputation Accuracy for <math>X_5</math> (Unobserved)</b>	0.8729	1.0

**Results and Analysis.** We analyze example (b) from Figure 3 (full results of observation ratio at 0.1 and 0.3 are in Appendix J.1). Table 1 shows that our model achieves near-perfect recovery for simple conjunctive rules ( $X_3, X_4$ ) and high imputation accuracy for the complex disjunctive rule ( $X_5$ ). Figure 4(a)-(b) illustrates stable training dynamics. For  $X_5$ , the model uses sequential covering (Figure 4(c)), with “well-explained” examples reducing the remaining set. The fine-tuning (FT) phase is followed, which corrects the rule structure and boosts accuracy (Figure 4(d)-(e)). The corresponding ablation study (Table 2) confirms that fine-tuning is critical for disjunctive rules, increasing unobserved imputation accuracy for  $X_5$  from 0.87 to 1.00.

Table 3: Impact of **rule optimization order** on learning progress. Use the example (a) of Figure 3. Note: ✓ denotes successful learning for the respective predicate.

Cycle	Metric	Run 1	Run 2	Run 3
Cycle 1	Optimization Order	$[X_5, X_4, X_3]$	$[X_3, X_5, X_4]$	$[X_3, X_4, X_5]$
	Rule Accu.	$X_3 \checkmark, X_4, X_5$	$X_3 \checkmark, X_4 \checkmark, X_5$	$X_3 \checkmark, X_4 \checkmark, X_5 \checkmark$
	Imputation Accu., Train Loss	$X_3 : 1.00, 0.005$ $X_4 : 0.87, 0.074$ $X_5 : 0.94, 0.053$	$X_3 : 1.00, 0.005$ $X_4 : 1.00, 0.004$ $X_5 : 0.94, 0.035$	$X_3 : 1.00, 0.005$ $X_4 : 1.00, 0.004$ $X_5 : 1.00, 0.003$
Cycle 2	Optimization Order	$[X_3, X_5, X_4]$	$[X_5, X_3, X_4]$	—
	Rule Accu.	$X_3 \checkmark, X_4 \checkmark, X_5$	$X_3 \checkmark, X_4 \checkmark, X_5 \checkmark$	—
	Imputation Accu., Train Loss	$X_3 : 1.00, 0.005$ $X_4 : 1.00, 0.004$ $X_5 : 0.94, 0.035$	$X_3 : 1.00, 0.005$ $X_4 : 1.00, 0.004$ $X_5 : 1.00, 0.003$	—
Cycle 3	Optimization Order	$[X_3, X_4, X_5]$	—	—
	Rule Accu.	$X_3 \checkmark, X_4 \checkmark, X_5 \checkmark$	—	—
	Imputation Accu., Train Loss	$X_3 : 1.00, 0.005$ $X_4 : 1.00, 0.004$ $X_5 : 1.00, 0.003$	—	—

Our asynchronous coordinate descent is robust to different rule optimization orders (Table 3, Appendix Figures 9-11) and is data-efficient, recovering complex rules with as few as 4,000 samples (Appendix Figure 8). While coordinate descent requires different cycle numbers, Appendix Table 9 demonstrate minimal time and memory costs.

**Convergence Analysis of Asynchronous Coordinate Descent.** Exact rule-set induction reduces to the minimum-set-cover problem (*NP-hard*), so like any practical rule learner, we do not claim global optimality. Instead, we frame search as asynchronous block-coordinate descent on a smooth surrogate loss: at each step, we update a single rule embedding in closed form, which guarantees the loss never increases yet keeps each move computationally cheap. To guard against poor local minima, we (i) freeze a rule only after this rule is perfectly learned, and (ii) launch diverse initializations. Across 20 runs on synthetic datasets (Tables 23-28), this strategy delivers  $< 1.3\%$  imputation performance variance, and the top-ranked learned rules consistently match ground truth rules. [More theoretical discussions are provided in Appendix B.](#)

## 6.2 REAL-WORLD DATA EXPERIMENTS

We validate our approach on three real-world datasets, comparing it with (i) *statistical models* (**MICE**(van Buuren & Groothuis-Oudshoorn, 2011), **MissForest**(Stekhoven & Bühlmann, 2012)), (ii) *deep generative models* (**MLP**, **GAIN**(Yoon et al., 2018), **MissDiff**(Ouyang et al., 2023),

432 **mDAE**(Dupuy et al., 2024), **VAE**(Veldkamp et al., 2025)) and *(iii) rule-based interpretable models*  
 433 **(BRCG**(Dash et al., 2018), **RRL**(Wang et al., 2021), **DR-NET**(Qiao et al., 2021), **LEN**(Barbiero  
 434 et al., 2022)). For each dataset, we randomly miss some features. We then evaluated the models  
 435 on their ability to impute these missing values, as well as their performance on a downstream target  
 436 classification task. Preprocessing and baselines details are provided in Appendix D.2 and D.3.

437  
438 Table 4: Comparison of imputation accuracy and learned rules on the Birds dataset.  
439

Method	Imp Acc.	Learned Rules
LEN	0.57	$abnormal\_bird \leftarrow (ostrich \wedge \neg wounded) \vee (bird \wedge wounded)$
	0.55	$can\_fly \leftarrow (bird \wedge \neg ostrich) \vee (\neg ostrich \wedge \neg wounded)$
RRL	0.53	$abnormal\_bird \leftarrow (bird \wedge \neg wounded) \vee (bird \wedge ostrich)$
	0.51	$can\_fly \leftarrow (\neg ostrich \wedge \neg wounded) \vee (bird \wedge \neg ostrich)$
BRCG	0.50	$abnormal\_bird \leftarrow bird \wedge ostrich$
	0.47	$can\_fly \leftarrow bird \wedge \neg abnormal\_bird$
DR-NET	0.56	$abnormal\_bird \leftarrow (bird \wedge \neg ostrich \wedge wounded) \vee (bird \wedge ostrich \wedge \neg wounded)$
	0.53	$can\_fly \leftarrow (bird \wedge \neg ostrich \wedge \neg abnormal\_bird) \vee (bird \wedge \neg ostrich \wedge \neg wounded)$
NS-FCN	<b>1.00</b>	$abnormal\_bird \leftarrow ostrich \vee (bird \wedge wounded)$
	<b>1.00</b>	$can\_fly \leftarrow bird \wedge \neg abnormal\_bird$

450  
451 Table 5: Comparison of imputation accuracy and learned rules on the Heart Disease dataset.  
452

Method	Imp Acc.	Learned Rules
LEN	0.65	$trestbps\_high \leftarrow (\neg st\_mild \wedge cp\_atypical\_angina) \vee (chol\_low \wedge cp\_asymptomatic)$
	0.53	$chol\_high \leftarrow (sex\_female \wedge ca\_2) \vee (bp\_normal \wedge cp\_asymptomatic)$
	0.62	$hr\_high \leftarrow (cp\_asymptomatic \wedge target) \vee (chol\_low \wedge ca\_1)$
	0.70	$st\_severe \leftarrow (cp\_non\_anginal \wedge \neg fbs\_normal) \vee (age\_old \wedge chol\_low)$
RRL	0.28	$trestbps\_high \leftarrow (sex\_female \wedge \neg cp\_typical\_angina) \vee (exang\_yes \wedge \neg thal\_normal)$
	0.33	$hr\_high \leftarrow (age\_middle \wedge sex\_male) \vee (\neg restecg\_stt\_abnormality \wedge slope\_upsloping)$
	0.33	$thalach \leftarrow (age < 60) \wedge (restecg = 0)$
	0.32	$st\_severe \leftarrow (\neg exang\_yes \wedge \neg slope\_flat) \vee (chol\_low \wedge cp\_asymptomatic)$
BRCG	0.53	$trestbps\_high \leftarrow \neg age\_young \wedge \neg ca\_4$
	0.35	$chol\_high \leftarrow \neg age\_young \wedge \neg restecg\_hypertrophy$
	0.33	$hr\_high \leftarrow \neg cp\_typical\_angina \wedge \neg ca\_4$
	0.32	$st\_severe \leftarrow \neg age\_young \wedge \neg slope\_upsloping$
DR-NET	0.53	$trestbps\_high \leftarrow (chol\_low \wedge \neg hr\_low \wedge \neg fbs\_high) \vee (slope\_flat \wedge ca\_1 \wedge thal\_normal)$
	0.33	$chol\_high \leftarrow sex\_male \wedge slope\_upsloping \wedge ca\_3$
	0.33	$hr\_high \leftarrow \neg age\_old \wedge \neg cp\_typical\_angina \wedge fbs\_high$
	0.32	$st\_severe \leftarrow hr\_high \wedge \neg sex\_male \wedge \neg fbs\_normal$
NS-FCN	<b>0.86</b>	$trestbps\_high \leftarrow (age > 60) \wedge (chol > 250)$
	<b>0.85</b>	$chol\_high \leftarrow (sex = 1 \wedge age > 55) \vee (trestbps > 150)$
	<b>0.90</b>	$hr\_high \leftarrow (trestbps > 145) \vee (age > 57 \wedge cp = 3)$
	<b>0.76</b>	$st\_severe \leftarrow (slope = 2) \wedge (thalach < 150)$

472 For *logical reasoning*, we used the Birds dataset (Tafjord et al., 2021) with a 90% missing ratio  
 473 for two key predicates. As shown in Table 4, under some random seeds, NS-FCN achieves per-  
 474 fect imputation accuracy (1.00) and, crucially, **perfectly recovers the ground truth logical rules**,  
 475 highlighting its superior capability in deciphering underlying logical structures. Table 6 compares  
 476 our approach with non-interpretable baselines. While a MLP achieve optimal performance given  
 477 the simplicity of the Birds dataset, our model remains highly competitive; more importantly, it  
 478 demonstrates robustness across diverse random initializations, successfully recovering the correct  
 479 ground-truth rules in the majority of cases. Table 20 further show that the a few hundred samples  
 480 are sufficient for the model to converge to the correct logical truth.

481 In *medical diagnosis*, we use Heart Disease (Detrano et al., 1989) and SPECT Heart (Kurgan et al.,  
 482 2001) datasets, introducing 30% missingness. We also vary the observation ratio from 0.3 to 0.9, and  
 483 the results in Tables 18 and 19 shows comparable performance with only 30% of the data observed.

484 On the Heart Disease dataset, with its mix of continuous and categorical features, NS-FCN’s direct  
 485 handling of continuous values led to superior imputation (e.g., 90% accuracy for *thalach*) and  
 the discovery of **clinically relevant rules with numerical thresholds** (e.g., *age > 60, chol > 250*),

as shown in Tables 5 and 32. NS-FCN attains imputation accuracy comparable to the advanced statistical and generative baselines, yet distinguishes itself by offering full interpretability, a critical advantage over these black-box approaches. Compared with rule-based models, our evaluation highlights NS-FCN’s unique ability to handle heterogeneous data types. A key distinction is that NS-FCN directly models continuous features, whereas **baseline methods are restricted to binary inputs**, forcing discretization (e.g., for `trestbps`, binning values into  $< 120$ ,  $120 - 140$ ,  $> 140$  mmHg as low, normal, and high).

On the binary SPECT dataset, we randomly miss all 22 features, thus we report the diagnosis accuracy after imputation. When the imputed features are used for diagnosis, NS-FCN outperforms all baselines on both Heart Disease and SPECT, as shown in Table 7. **Unlike baseline models that train a classifier on previously imputed samples, where imputation errors inevitably propagate to the downstream task, our method jointly optimizes rule discovery and target inference.** Furthermore, our use of soft-logic relaxation prevents the model from overfitting to noise (such as incorrect features), enabling it to capture dominant logical structures. This robustness is further supported by the comprehensive noise sensitivity analysis in Appendix I.1 (Tables 16 and 17), which demonstrates that the model learns valid rule approximations (e.g. capturing one correct clause) and maintains strong predictive performance even as noise levels increase.

Detailed rules and LLM assessments are in Appendix Tables 30, 31, and 32.

Table 6: Imputation accuracy of missing feature value comparison across Heart Disease and Bird datasets on non-interpretable baselines. Results are over 10 random seeds.

Method	Heart Disease				Birds	
	<code>trestbps</code>	<code>chol</code>	<code>thalach</code>	<code>oldpeak</code>	<code>abnormal_bird</code>	<code>can_fly</code>
MICE	0.84 $\pm$ 0.016	0.83 $\pm$ 0.014	0.88 $\pm$ 0.011	0.87 $\pm$ 0.015	0.88 $\pm$ 0.006	0.86 $\pm$ 0.011
MissForest	<b>0.88<math>\pm</math>0.015</b>	0.84 $\pm$ 0.012	<b>0.91<math>\pm</math>0.004</b>	0.88 $\pm$ 0.016	0.38 $\pm$ 0.123	0.68 $\pm$ 0.086
MLP	<b>0.88<math>\pm</math>0.009</b>	<b>0.85<math>\pm</math>0.016</b>	0.88 $\pm$ 0.014	0.80 $\pm$ 0.025	<b>0.96<math>\pm</math>0.059</b>	<b>0.99<math>\pm</math>0.003</b>
GAIN	0.85 $\pm$ 0.022	0.84 $\pm$ 0.011	0.90 $\pm$ 0.014	<b>0.89<math>\pm</math>0.014</b>	0.83 $\pm$ 0.102	0.82 $\pm$ 0.083
MissDiff	0.82 $\pm$ 0.017	0.83 $\pm$ 0.019	0.89 $\pm$ 0.018	0.84 $\pm$ 0.030	0.83 $\pm$ 0.020	0.86 $\pm$ 0.007
mDAE	<b>0.88<math>\pm</math>0.011</b>	0.84 $\pm$ 0.012	0.90 $\pm$ 0.015	0.87 $\pm$ 0.015	0.87 $\pm$ 0.002	0.87 $\pm$ 0.004
VAE-based	0.85 $\pm$ 0.015	0.84 $\pm$ 0.021	0.90 $\pm$ 0.015	0.86 $\pm$ 0.015	0.62 $\pm$ 0.006	0.87 $\pm$ 0.004
<b>NS-FCN</b>	0.87 $\pm$ 0.025	<b>0.85<math>\pm</math>0.017</b>	0.88 $\pm$ 0.014	0.78 $\pm$ 0.020	0.95 $\pm$ 0.064	0.95 $\pm$ 0.064

Table 7: Medical diagnosis after missing value imputation. Results are over 10 random seeds.

Method	Heart Disease		SPECT	
	Accuracy	<i>F1</i>	Accuracy	<i>F1</i>
MICE(van Buuren & Groothuis-Oudshoorn, 2011)	0.83 $\pm$ 0.010	0.81 $\pm$ 0.012	0.78 $\pm$ 0.019	0.87 $\pm$ 0.013
MissForest(Stekhoven & Bühlmann, 2012)	0.83 $\pm$ 0.013	0.81 $\pm$ 0.014	0.79 $\pm$ 0.012	0.87 $\pm$ 0.008
MLP	0.84 $\pm$ 0.010	0.82 $\pm$ 0.012	<b>0.92<math>\pm</math>0.007</b>	0.90 $\pm$ 0.005
GAIN(Yoon et al., 2018)	0.84 $\pm$ 0.004	0.82 $\pm$ 0.006	0.76 $\pm$ 0.019	0.85 $\pm$ 0.013
MissDiff(Ouyang et al., 2023)	0.84 $\pm$ 0.010	0.82 $\pm$ 0.011	0.77 $\pm$ 0.023	0.86 $\pm$ 0.016
mDAE(Dupuy et al., 2024)	0.84 $\pm$ 0.009	0.82 $\pm$ 0.010	0.80 $\pm$ 0.013	0.88 $\pm$ 0.009
VAE-based(Veldkamp et al., 2025)	0.83 $\pm$ 0.009	0.81 $\pm$ 0.009	0.75 $\pm$ 0.016	0.85 $\pm$ 0.011
BRCG(Dash et al., 2018)	0.77 $\pm$ 0.006	0.74 $\pm$ 0.034	0.85 $\pm$ 0.046	0.90 $\pm$ 0.035
RRL(Wang et al., 2021)	0.78 $\pm$ 0.002	0.80 $\pm$ 0.003	0.90 $\pm$ 0.005	0.94 $\pm$ 0.005
DR-NET(Qiao et al., 2021)	0.85 $\pm$ 0.005	0.82 $\pm$ 0.005	0.89 $\pm$ 0.025	0.92 $\pm$ 0.017
LEN(Barbiero et al., 2022)	0.69 $\pm$ 0.007	0.80 $\pm$ 0.000	0.76 $\pm$ 0.035	0.85 $\pm$ 0.017
<b>NS-FCN</b>	<b>0.91<math>\pm</math>0.009</b>	<b>0.91<math>\pm</math>0.009</b>	<b>0.92<math>\pm</math>0.009</b>	<b>0.96<math>\pm</math>0.009</b>

## 7 CONCLUSION

Our NS-FCN framework effectively learns interpretable rules for missing value imputation, demonstrating strong performance across a diverse range of synthetic and real-world datasets. A key strength is its ability to seamlessly reason over heterogeneous data, handling both binary predicates (e.g., Birds) and continuous features in complex domains like medical diagnosis (SPECT, Heart Disease). It successfully handles missing data and learns hierarchical rule structures, offering significant potential for trustworthy diagnostics and transparent decision-making.

540 REPRODUCIBILITY STATEMENT  
541

542 We have made extensive efforts to ensure the reproducibility of our results. The complete description  
543 of both synthetic dataset generation and real-world dataset preprocessing methods are illustrated in  
544 Appendix E and D.2. Details of the computational setup, including hardware configuration and  
545 software environment, as well as the choice of hyper-parameters are documented in Appendix J.4  
546 and K.3. We will release our code in the camera-ready stage to facilitate replication and further  
547 research.

548 REFERENCES  
549

550 Pietro Barbiero, Gabriele Ciravegna, Francesco Giannini, Pietro Lió, Marco Gori, and Stefano  
551 Melacci. Entropy-based logic explanations of neural networks. In *Proceedings of the AAAI  
552 Conference on Artificial Intelligence*, volume 36, pp. 6046–6054, 2022.

553 Dimitri P Bertsekas. Nonlinear programming. *Journal of the Operational Research Society*, 48(3):  
554 334–334, 1997.

555 Antoine Bordes, Nicolas Usunier, Alberto Garcia-Duran, Jason Weston, and Oksana Yakhnenko.  
556 Translating embeddings for modeling multi-relational data. In *Advances in Neural Information  
557 Processing Systems*, volume 26, 2013.

559 Andres Campero, Aldo Pareja, Tim Klinger, Josh Tenenbaum, and Sebastian Riedel. Logical rule  
560 induction and theory learning using neural theorem proving. *arXiv preprint arXiv:1809.02193*,  
561 2018.

562 Zhi Chen, Sarah Tan, Urszula Chajewska, Cynthia Rudin, and Rich Caruna. Missing values and  
563 imputation in healthcare data: Can interpretable machine learning help? In *Conference on Health,  
564 Inference, and Learning*, pp. 86–99. PMLR, 2023.

566 Xueling Feng, Paul Weng, Matthieu Zimmer, Dong Li, Wulong Liu, Jianye Hao, Claire Glanois, Zhao-  
567 hui Jiang. Neuro-symbolic hierarchical rule induction. In *International Conference on Machine  
568 Learning (ICML)*, pp. 7583–7615. PMLR, 2022.

569 William W Cohen. Fast effective rule induction. In *Machine learning proceedings 1995*, pp. 115–  
570 123. Elsevier, 1995.

572 Andrew Cropper and Rolf Morel. Learning programs by learning from failures. *Machine Learning*,  
573 110(4):801–856, 2021.

575 Sanjeeb Dash, Oktay Gunluk, and Dennis Wei. Boolean decision rules via column generation.  
576 *Advances in neural information processing systems*, 31, 2018.

577 Robert Detrano, Andras Janosi, Walter Steinbrunn, Matthias Pfisterer, Johann-Jakob Schmid, Sar-  
578 bjit Sandhu, Kern H Guppy, Stella Lee, and Victor Froelicher. International application of a  
579 new probability algorithm for the diagnosis of coronary artery disease. *The American journal of  
580 cardiology*, 64(5):304–310, 1989.

582 Honghua Dong, Jiayuan Mao, Tian Lin, Chong Wang, Lihong Li, and Denny Zhou. Neural logic  
583 machines. *arXiv preprint arXiv:1904.11694*, 2019.

584 Mariette Dupuy, Marie Chavent, and Remi Dubois. mdae: modified denoising autoencoder for  
585 missing data imputation. *arXiv preprint arXiv:2411.12847*, 2024.

587 Bradley Efron. Missing data, imputation, and the bootstrap. *Journal of the American Statistical  
588 Association*, 89(426):463–475, 1994.

590 Khaled M Fouad, Mahmoud M Ismail, Ahmad Taher Azar, and Mona M Arafa. Advanced methods  
591 for missing values imputation based on similarity learning. *PeerJ Computer Science*, 7:e619,  
592 2021.

593 Kelvin Guu, John Miller, and Percy Liang. Traversing knowledge graphs in vector space. *arXiv  
preprint arXiv:1506.01094*, 2015.

594 Pascal Hitzler and Md Kamruzzaman Sarker. Neuro-symbolic artificial intelligence: The state of  
 595 the art. 2022.

596

597 Diederik P Kingma and Max Welling. Auto-encoding variational bayes. *arXiv preprint*  
 598 *arXiv:1312.6114*, 2013.

599 Lukasz A Kurgan, Krzysztof J Cios, Ryszard Tadeusiewicz, Marek Ogiela, and Lucy S Goodenday.  
 600 Knowledge discovery approach to automated cardiac spect diagnosis. *Artificial intelligence in*  
 601 *medicine*, 23(2):149–169, 2001.

602

603 Linchao Li, Bowen Du, Yonggang Wang, Lingqiao Qin, and Huachun Tan. Estimation of missing  
 604 values in heterogeneous traffic data: Application of multimodal deep learning model. *Knowledge-  
 605 Based Systems*, 194:105592, 2020.

606 Yankai Lin, Zhiyuan Liu, Maosong Sun, Yang Liu, and Xuan Zhu. Learning entity and relation em-  
 607 beddings for knowledge graph completion. In *Proceedings of the AAAI Conference on Artificial*  
 608 *Intelligence*, volume 29, 2015.

609

610 Robin Manhaeve, Sebastian Dumancic, Angelika Kimmig, Thomas Demeester, and Luc De Raedt.  
 611 DeepProbLog: Neural probabilistic logic programming. *Advances in neural information process-  
 612 ing systems*, 31, 2018.

613 Rahul Mazumder, Trevor Hastie, and Robert Tibshirani. Spectral regularization algorithms for learn-  
 614 ing large incomplete matrices. *The Journal of Machine Learning Research*, 11:2287–2322, 2010.

615

616 Yurii Nesterov. *Introductory lectures on convex optimization: A basic course*, volume 87. Springer  
 617 Science & Business Media, 2013.

618 Alessandro Oltramari, Jonathan Francis, Cory Henson, Kaixin Ma, and Ruwan Wickramarachchi.  
 619 Neuro-symbolic architectures for context understanding. In *Knowledge Graphs for Explainable*  
 620 *Artificial Intelligence: Foundations, Applications and Challenges*, pp. 143–160. IOS Press, 2020.

621

622 Yidong Ouyang, Liyan Xie, Chongxuan Li, and Guang Cheng. Missdiff: Training diffusion models  
 623 on tabular data with missing values. *arXiv preprint arXiv:2307.00467*, 2023.

624

625 Leonardo Pellegrina and Fabio Vandin. Scalable rule lists learning with sampling. In *Proceedings of*  
 626 *the 30th ACM SIGKDD Conference on Knowledge Discovery and Data Mining*, pp. 2352–2363,  
 627 2024.

628

629 Litao Qiao, Weijia Wang, and Bill Lin. Learning accurate and interpretable decision rule sets from  
 630 neural networks. In *Proceedings of the AAAI Conference on Artificial Intelligence*, volume 35,  
 631 pp. 4303–4311, 2021.

632

633 J. Ross Quinlan. Learning logical definitions from relations. *Machine learning*, 5:239–266, 1990.

634

635 Md Geaur Rahman and Md Zahidul Islam. A decision tree-based missing value imputation technique  
 636 for data pre-processing. In *The 9th Australasian Data Mining Conference: AusDM 2011*, pp. 41–  
 637 50. Australian Computer Society Inc, 2011.

638

639 Md Geaur Rahman and Md Zahidul Islam. Fimus: A framework for imputing missing values using  
 640 co-appearance, correlation and similarity analysis. *Knowledge-Based Systems*, 56:311–327, 2014.

641

642 Matthew Richardson and Pedro Domingos. Markov logic networks. *Machine learning*, 62:107–136,  
 643 2006.

644

645 Peter Richtárik and Martin Takáč. Iteration complexity of randomized block-coordinate descent  
 646 methods for minimizing a composite function. *Mathematical Programming*, 144(1):1–38, 2014.

647

648 Tim Rocktäschel and Sebastian Riedel. End-to-end differentiable proving. *Advances in neural*  
 649 *information processing systems*, 30, 2017.

650

651 Hikaru Shindo, Masaaki Nishino, and Akihiro Yamamoto. Differentiable inductive logic program-  
 652 ming for structured examples. In *Proceedings of the AAAI Conference on Artificial Intelligence*,  
 653 volume 35, pp. 5034–5041, 2021.

648 Daniel J Stekhoven and Peter Bühlmann. Missforest—non-parametric missing value imputation for  
 649 mixed-type data. *Bioinformatics*, 28(1):112–118, 2012.

650

651 Lena Stempfle and Fredrik Johansson. Minty: Rule-based models that minimize the need for im-  
 652 puting features with missing values. In *International Conference on Artificial Intelligence and*  
 653 *Statistics*, pp. 964–972. PMLR, 2024.

654 Oyvind Tafjord, Bhavana Dalvi, and Peter Clark. Proofwriter: Generating implications, proofs, and  
 655 abductive statements over natural language. In *Findings of the Association for Computational*  
 656 *Linguistics: ACL-IJCNLP 2021*, pp. 3621–3634, 2021.

657

658 Théo Trouillon, Johannes Welbl, Sebastian Riedel, Éric Gaussier, and Guillaume Bouchard. Com-  
 659 plex embeddings for simple link prediction. In *International conference on machine learning*, pp.  
 660 2071–2080. PMLR, 2016.

661 Paul Tseng. Convergence of a block coordinate descent method for nondifferentiable minimization.  
 662 *Journal of optimization theory and applications*, 109(3):475–494, 2001.

663

664 Stef van Buuren and Catharina Gerarda Maria Groothuis-Oudshoorn. mice: Multivariate imputation  
 665 by chained equations in r. *Journal of statistical software*, 45(3), 2011.

666 Karel Veldkamp, Raoul Grasman, and Dylan Molenaar. Handling missing data in variational autoen-  
 667 coder based item response theory. *British Journal of Mathematical and Statistical Psychology*, 78  
 668 (1):378–397, 2025.

669

670 Xinyu Wang, Isil Dillig, and Rishabh Singh. Synthesis of data completion scripts using finite tree  
 671 automata. *Proceedings of the ACM on Programming Languages*, 1(OOPSLA):1–26, 2017.

672

673 Zhen Wang, Jianwen Zhang, Jianlin Feng, and Zheng Chen. Knowledge graph embedding by trans-  
 674 lating on hyperplanes. In *Proceedings of the AAAI Conference on Artificial Intelligence*, vol-  
 675 ume 28, 2014. doi: 10.1609/aaai.v28i1.8870. URL <https://doi.org/10.1609/aaai.v28i1.8870>.

676

677 Zhuo Wang, Wei Zhang, Ning Liu, and Jianyong Wang. Scalable rule-based representation learning  
 678 for interpretable classification. *Advances in Neural Information Processing Systems*, 34:30479–  
 679 30491, 2021.

680

681 Dennis Wei, Sanjeeb Dash, Tian Gao, and Oktay Gunluk. Generalized linear rule models. In  
 682 *International conference on machine learning*, pp. 6687–6696. PMLR, 2019.

683

684 Stephen J Wright. Coordinate descent algorithms. *Mathematical programming*, 151(1):3–34, 2015.

685

686 Yang Yang, Chao Yang, Boyang Li, Yinghao Fu, and Shuang Li. Neuro-symbolic temporal point  
 687 processes. *arXiv preprint arXiv:2406.03914*, 2024.

688

689 Jinsung Yoon, James Jordon, and Mihaela Schaar. Gain: Missing data imputation using generative  
 690 adversarial nets. In *International conference on machine learning*, pp. 5689–5698. PMLR, 2018.

691

692 Chengqi Zhang, Yongsong Qin, Xiaofeng Zhu, Jilian Zhang, and Shichao Zhang. Clustering-based  
 693 missing value imputation for data preprocessing. In *2006 4th IEEE International Conference on*  
 694 *Industrial Informatics*, pp. 1081–1086. IEEE, 2006.

695

696

697

698

699

700

701

702 A RELATED WORK SUPPLEMENT  
703  
704  
705  
706

707 **Traditional Inductive Logic Programming (ILP) Methods.** Inductive Logic Programming learns  
708 logical rules from relational data. Cohen (1995) proposed RIPPER, a fast rule induction algorithm  
709 using separate-and-conquer strategy. Quinlan (1990) developed FOIL, which generates clauses it-  
710 eratively. Dash et al. (2018) introduced Boolean decision rules using column generation. Wei et al.  
711 (2019) proposed GLRM integrating decision rules into linear models. Cropper & Morel (2021)  
712 presented LFF implemented in Popper. These approaches rely on heuristics but may not guarantee  
713 optimal solutions. Pellegrina & Vandin (2024) proposed SamRuLe for near-optimal rule lists via  
714 sampling.

715 **Differentiable ILP Methods.** Traditional ILP models struggle with noisy data and scalability. Dif-  
716 ferentiable approaches address these issues by integrating continuous relaxation, which allows gra-  
717 dient descent for optimization. Shindo et al. (2021) proposed  $\partial$ ILP, which represents logic rules in  
718 a differentiable form and combines neural networks with symbolic logic. Manhaeve et al. (2018) in-  
719 troduced DeepProbLog, extending ProbLog with neural predicates. Neural Logic Machines (NLMs)  
720 (Dong et al., 2019) combine MLPs with logic programming to improve computational efficiency but  
721 reduce interpretability.

722 **Broader Missing Data Imputation Methods.** Missing data imputation methods range from global  
723 model-based techniques to localized and hybrid strategies, extending to deep and ensemble frame-  
724 works.

725 At the global end, nonparametric bootstrap methods (Efron, 1994) provide bias-corrected estimates  
726 via repeated sampling, while spectral regularization approaches like SOFT-IMPUTE (Mazumder  
727 et al., 2010) solve a nuclear-norm minimization through iterative soft-thresholded SVD. **Classi-**  
728 **cal multivariate imputation schemes such as MICE** (van Buuren & Groothuis-Oudshoorn, 2011)  
729 **construct a sequence of conditional models for each variable with missingness and iteratively sam-**  
730 **ple from these chained regressions until convergence, thereby approximating draws from the joint**  
731 **posterior and naturally propagating uncertainty across multiple imputations.** Tree-based ensemble  
732 **methods such as MissForest** (Stekhoven & Bühlmann, 2012) **adopt an iterative refinement strategy**  
733 **in which random forests are trained per variable using the currently imputed data as predictors,**  
734 **updating missing entries via out-of-bag predictions until changes stabilize, thus capturing complex**  
735 **nonlinearities and high-order interactions without requiring parametric distributional assumptions.**

736 Moving toward local adaptation, decision tree-based EM (DMI) (Rahman & Islam, 2011) partitions  
737 complete cases via C4.5 and imputes within each leaf, and clustering-based random imputation  
738 (CRI) (Zhang et al., 2006) applies kernel-weighted estimation in the nearest k-means cluster. Hybrid  
739 similarity learners, such as KI and its fuzzy extension FCKI (Fouad et al., 2021), refine this idea by  
740 dynamically selecting neighborhood sizes before multivariate imputation. For high-dimensional or  
741 heterogeneous data, deep architectures like **GAIN** (Yoon et al., 2018) **cast imputation as a generative**  
742 **adversarial game where a generator proposes imputations conditioned on an observed-mask vector**  
743 **and a discriminator learns to distinguish observed from imputed components, while VAE-based**  
744 **imputers** (Veldkamp et al., 2025) **treat the complete feature matrix as generated from low-dimensional**  
745 **latent variables and learn to reconstruct missing entries via amortized variational inference under**  
746 **a probabilistic encoder-decoder architecture.** Building on denoising autoencoders, **mDAE** (Dupuy  
747 et al., 2024) **modifies the reconstruction loss to ignore pre-imputed values at missing positions and**  
748 **couples this with an overcomplete hidden representation, which empirically improves RMSE over**  
749 **standard DAEs and several classical imputers across multiple UCI datasets** (Dupuy et al., 2024). In  
750 the same spirit of generative modeling, **MissDiff** (Ouyang et al., 2023) **trains a diffusion model on**  
751 **tabular data with missing values by injecting noise along a forward stochastic process and learning**  
752 **a reverse denoising process that is explicitly conditioned on the observed-mask pattern, thereby pro-**  
753 **ducing imputations through iterative refinement from pure noise.** Models such as **MMDL** (Li et al.,  
754 2020) align stacked autoencoder embeddings across modalities to exploit cross-view correlations.  
755 Ensemble schemes like **FIMUS** (Rahman & Islam, 2014) combine co-appearance, correlation, and  
similarity in a weighted-voting framework. Despite their varied focuses—ranging from global  
inference to localized and multimodal learning—these methods uniformly rely on statistical patterns  
and *do not leverage explicit logical rules to govern inter-variable relationships*.

## 756 B CONVERGENCE ANALYSIS OF COORDINATE GRADIENT DESCENT

757 For clarity, we analyze a simplified version of our learning algorithm in which each head predicate  
 758  $U_j$  is associated with a single parameter block  $\Theta_j$ . Let  $\Theta = (\Theta_1, \dots, \Theta_m)$  collect all parameters.  
 759 The global training objective is

$$760 \quad \mathcal{L}(\Theta) = \sum_{j=1}^m \mathcal{L}_{U_j}(\Theta), \quad \mathcal{L}_{U_j}(\Theta) = \text{mean}((v_{U_j}(\Theta) \odot \text{mask}_j - U_{j,\text{obs}} \odot \text{mask}_j)^2), \quad (7)$$

761 where  $v_{U_j}(\Theta)$  is computed by forward chaining using the differentiable operators introduced in the  
 762 main text (e.g., Eq. 4).

### 763 B.1 ASSUMPTIONS

764 We make the following standard assumptions for smooth block coordinate descent (e.g., (Tseng,  
 765 2001; Bertsekas, 1997; Nesterov, 2013))

766 **Assumption 1** *The objective  $\mathcal{L} : \mathbb{R}^d \rightarrow \mathbb{R}$  is*

- 767 1. *bounded below:  $\inf_{\Theta} \mathcal{L}(\Theta) > -\infty$ ,*
- 768 2. *continuously differentiable in  $\Theta$ , and*
- 769 3. *has block-wise Lipschitz-continuous gradients: for each  $j$  there exists  $L_j < \infty$  such that,  
 770 for all  $\Theta$  and all  $h_j$ ,*

$$771 \quad \|\nabla_{\Theta_j} \mathcal{L}(\Theta + e_j h_j) - \nabla_{\Theta_j} \mathcal{L}(\Theta)\| \leq L_j \|h_j\|, \quad (8)$$

772 where  $e_j h_j$  denotes the vector obtained by changing only block  $j$ .

773 These conditions hold in our setting because  $\mathcal{L}$  is built from smooth operations (e.g., linear maps,  
 774 sigmoid, softmax, log-sum-exp) composed with a squared loss, and training is restricted to bounded  
 775 level sets.

### 776 B.2 IDEALIZED FULL-BATCH BLOCK COORDINATE GRADIENT DESCENT

777 Consider the following idealized algorithm. At iteration  $t$  we pick a block index  $j_t \in \{1, \dots, m\}$   
 778 (e.g., by cycling through  $\{1, \dots, m\}$ ) and perform a gradient step on that block only:

$$779 \quad \Theta_{j_t}^{t+1} = \Theta_{j_t}^t - \eta \nabla_{\Theta_{j_t}} \mathcal{L}(\Theta^t), \quad (9)$$

$$780 \quad \Theta_{\ell}^{t+1} = \Theta_{\ell}^t \quad \text{for all } \ell \neq j_t, \quad (10)$$

781 where  $\eta > 0$  is a step size. This matches the idealized version of the rule update in Section 5.1:  
 782 when we update  $U_{j_t}$ , all other predicates  $U_{\ell}$  are kept fixed.

783 **Lemma 1 (Monotone decrease for small steps)** *Suppose Assumption 1 holds. If the step size sat-  
 784 isfies  $0 < \eta \leq 1/L_{j_t}$  at iteration  $t$ , then*

$$785 \quad \mathcal{L}(\Theta^{t+1}) \leq \mathcal{L}(\Theta^t) - \frac{\eta}{2} \|\nabla_{\Theta_{j_t}} \mathcal{L}(\Theta^t)\|^2. \quad (11)$$

786 In particular, the sequence  $\{\mathcal{L}(\Theta^t)\}_{t \geq 0}$  is monotonically non-increasing and convergent.

787 **Proof 1 (Proof sketch)** *By block-wise Lipschitz continuity of  $\nabla_{\Theta_{j_t}} \mathcal{L}$ ,*

$$788 \quad \mathcal{L}(\Theta^{t+1}) = \mathcal{L}(\Theta^t + e_{j_t}(\Theta_{j_t}^{t+1} - \Theta_{j_t}^t)) \quad (12)$$

$$789 \quad \leq \mathcal{L}(\Theta^t) + \langle \nabla_{\Theta_{j_t}} \mathcal{L}(\Theta^t), \Theta_{j_t}^{t+1} - \Theta_{j_t}^t \rangle + \frac{L_{j_t}}{2} \|\Theta_{j_t}^{t+1} - \Theta_{j_t}^t\|^2. \quad (13)$$

790 *Substituting the update  $\Theta_{j_t}^{t+1} - \Theta_{j_t}^t = -\eta \nabla_{\Theta_{j_t}} \mathcal{L}(\Theta^t)$  and rearranging gives*

$$791 \quad \mathcal{L}(\Theta^{t+1}) \leq \mathcal{L}(\Theta^t) - \eta \left(1 - \frac{\eta L_{j_t}}{2}\right) \|\nabla_{\Theta_{j_t}} \mathcal{L}(\Theta^t)\|^2. \quad (14)$$

792 If  $\eta \leq 1/L_{j_t}$ , then  $1 - \eta L_{j_t}/2 \geq 1/2$ , yielding the claimed inequality.

793 Lemma 1 implies that the loss decreases at every iteration and the gradients on updated blocks cannot  
 794 stay large forever. Combined with a mild assumption that each block is selected infinitely often, we  
 795 obtain convergence to a block-stationary point.

810  
 811 **Proposition 1 (Convergence to a block-stationary point)** *Assume 1 holds, the level set  $\{\Theta : \mathcal{L}(\Theta) \leq \mathcal{L}(\Theta^0)\}$  is bounded, each block  $j$  is selected infinitely often, and the step sizes satisfy  $0 < \eta \leq \min_j 1/L_j$ . Then any limit point  $\Theta^*$  of the sequence  $\{\Theta^t\}$  generated by the above block coordinate gradient method is block-stationary:*

$$\nabla_{\Theta_j} \mathcal{L}(\Theta^*) = 0 \quad \text{for all } j = 1, \dots, m. \quad (15)$$

812 *Equivalently, no single block  $\Theta_j$  can be perturbed to decrease  $\mathcal{L}$  while all other blocks are fixed.*

813  
 814 **Proof 2 (Proof sketch)** *Summing the inequality from Lemma 1 over  $t$  shows that*

$$\sum_{t=0}^{\infty} \|\nabla_{\Theta_{j_t}} \mathcal{L}(\Theta^t)\|^2 < \infty,$$

815 *so the block gradients must tend to zero along the subsequence where a given block  $j$  is updated.*  
 816 *Since each block is selected infinitely often and the iterates remain in a bounded level set, standard*  
 817 *arguments for block coordinate descent (Tseng, 2001) imply that any limit point has zero gradient*  
 818 *in every block.*

819 Thus, in the ideal full-batch setting with sufficiently small steps, our predicate-wise coordinate up-  
 820 dates produce a non-increasing loss sequence  $\{\mathcal{L}(\Theta^t)\}$  and converge to a point where no single  
 821 predicate block  $\Theta_j$  can further reduce the global objective.

### 822 B.3 STOCHASTIC MINI-BATCH VARIANT AND ADAM

823 In practice, our implementation uses mini-batches and the Adam optimizer for each block update (as  
 824 described in Section 5.1). In this case, the gradient  $\nabla_{\Theta_j} \mathcal{L}$  is replaced by a stochastic estimate com-  
 825 puted on a mini-batch, and the step uses Adam’s adaptive preconditioning. This yields a *stochastic*  
 826 block-coordinate gradient scheme: the loss is no longer guaranteed to decrease at every single up-  
 827 date, but under standard assumptions stochastic block-coordinate methods are known to approach  
 828 a neighborhood of a stationary point in expectation (see, e.g., (Richtárik & Takáč, 2014; Wright,  
 829 2015)).

## 830 C MODEL SUPPLEMENT DESCRIPTION

### 831 C.1 OPTIMIZATION DETAILS

832 Throughout all training stages, each rule embedding (or set of embeddings during joint fine-tuning)  
 833 is optimized using the Adam optimizer. A crucial step following each gradient update is the normal-  
 834 ization of the rule embeddings. This involves applying a Rectified Linear Unit (ReLU) activation to  
 835 the embedding data (ensuring non-negative values, which can aid interpretability for positive pred-  
 836 icate contributions) followed by  $L_2$  normalization of each row vector within the rule embedding  
 837 matrix. This normalization helps stabilize the training process and maintains consistent magnitudes  
 838 for the embedding components.

## 839 D DATASETS AND BASELINES

### 840 D.1 DATASETS

841 **Heart Disease.** We use the widely-cited Cleveland Clinic dataset from the UCI Heart Disease  
 842 database (Detrano et al., 1989). This dataset contains 303 patient records, each with 13 features—a  
 843 mix of continuous and categorical variables—such as age, cholesterol level, and resting blood pres-  
 844 sure. The task is to predict the presence of heart disease, which is indicated by the target variable on  
 845 a scale from 0 (absence) to 4 (severe). Following standard practice, we simplify this into a binary  
 846 classification problem: predicting presence (values 1-4) versus absence (value 0).

847 **SPECT.** The SPECT (Single Proton Emission Computed Tomography) dataset presents a binary  
 848 classification task to diagnose cardiac conditions (normal/abnormal) based on 22 binary patient fea-  
 849 tures. The dataset describes the diagnosis of cardiac SPECT images. Each of the patients is classified  
 850 into two categories: normal and abnormal. The 267 SPECT image sets (patients) database were pro-  
 851 cessed to extract features that summarize the original SPECT images. As a result, 44 continuous  
 852 feature patterns were created for each patient. The pattern was further processed to obtain 22 binary  
 853 feature patterns. The CLIP3 algorithm was used to generate classification rules from these patterns  
 854 (Kurgan et al., 2001). The CLIP3 algorithm generated rules that were 84.0% accurate (as compared

with cardiologists' diagnoses). A key challenge in this domain is the prevalence of missing data, making it an ideal testbed for our model's imputation and rule-learning capabilities.

**Birds.** Bird’s Rulebase is a well-known logic problem designed to assess an AI’s ability to learn and reason with hierarchical logical rules that mimic common-sense knowledge (Tafjord et al., 2021). It has the ground truth single theory of six rules<sup>1</sup> as follows.

```

can_fly(X) ← bird(X), not abnormal_bird(X)
bird(X) ← ostrich(X)
abnormal_bird(X) ← ostrich(X)
not can_fly(X) ← ostrich(X)
abnormal_bird(X) ← bird(X), wounded(X)
not can_fly(X) ← wounded(X)

```

Figure 5 further illustrates the structure of these rules.

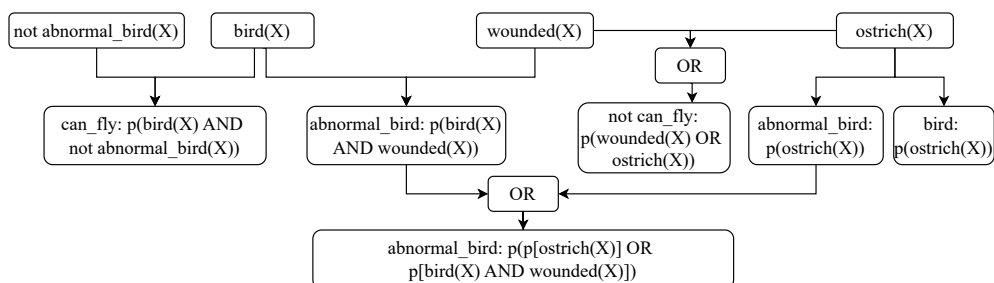


Figure 5: Ground truth rules for Bird dataset.

## D.2 PREPROCESSING OF DATASETS

**Heart Disease.** The UCI Heart Disease dataset contains a mix of 13 continuous and categorical features with 303 samples. To create a challenging imputation task, we introduced a 30% missing ratio independently into four key continuous variables: resting blood pressure (`trestbps`), cholesterol (`chol`), maximum heart rate (`thalach`), and ST depression (`oldpeak`). Following the protocol in MissDiff(Ouyang et al., 2023), we generate missing values under a Missing Completely At Random (MCAR) mechanism. Let  $\mathbf{x} \in \mathbb{R}^d$  denote the complete data vector. We generate a binary mask vector  $\mathbf{m} \in \{0, 1\}^d$ , where  $m_i = 1$  indicates that  $x_i$  is observed, and  $m_i = 0$  indicates it is missing. The observed data is represented as  $\tilde{\mathbf{x}} = \mathbf{x} \odot \mathbf{m} + \mathbf{n} \mathbf{a} \odot (1 - \mathbf{m})$ , where  $\odot$  denotes element-wise multiplication.

For our NS-FCN framework, the task is to directly impute these missing continuous values. For deep learning baselines, continuous features are standardized using Z-score normalization, and categorical features are one-hot encoded. For tree-based and statistical baselines (MissForest, MICE), categorical variables are treated as factors. However, to accommodate the baseline models which only support binary inputs, we first discretized these four variables into three categorical bins based on clinical thresholds: blood pressure ( $< 120$ ,  $120 - 140$ ,  $> 140$ ), cholesterol ( $< 200$ ,  $200 - 240$ ,  $\geq 240$ ), max heart rate ( $< 100$ ,  $100 - 160$ ,  $\geq 160$ ), and ST depression ( $\leq 1.0$ ,  $1.0 - 2.0$ ,  $> 2.0$ ). The baselines were then tasked with imputing the correct category. Consequently, we evaluate the imputation accuracy on the discretized bins.

**SPECT Heart.** The dataset's 22 binary features were randomly masked with a 30% probability to simulate missing data. Our framework was then applied to a two-stage task: first, to impute the missing features, and second, to perform the final patient diagnosis based on the completed feature set. The diagnostic performance is compared against five baseline methods, including four rule-based approaches and an MLP.

**Birds.** Following the ground truth logical rules, we generated a dataset of 1,500 samples. To create a difficult logical reasoning challenge, we introduced a 90% missing ratio for two crucial latent

<sup>1</sup><https://www.doc.ic.ac.uk/~mjs/teaching/KnowledgeRep491/ExtendedLP%20491-2x1.pdf>, p5

918 predicates: `can_fly` and `abnormal_bird`. The task for all models was to impute these missing  
 919 binary values based on the observed predicates. The imputation accuracy is compared against the  
 920 same set of baselines.

### 921 D.3 BASELINE MODELS

923 To rigorously evaluate performance, we compare our method against 11 established baselines, ranging  
 924 from classical statistical methods, to advanced deep generative models, and interpretable models.

#### 925 Statistical Models.

- 927 • **MICE** (van Buuren & Groothuis-Oudshoorn, 2011)

928 Multivariate Imputation by Chained Equations (MICE) is a widely used statistical method  
 929 based on Fully Conditional Specification (FCS). It iteratively imputes missing values by  
 930 modeling each feature with missing data as a function of other features using linear re-  
 931 gression (for continuous variables) or logistic regression (for categorical variables). We  
 932 generate  $m = 5$  imputed datasets and report results from the first completion.

- 933 • **MissForest** (Stekhoven & Bühlmann, 2012)

934 MissForest is a non-parametric method that handles mixed-type data using an iterative Ran-  
 935 dom Forest approach. It treats the missing data problem as a prediction task, training a ran-  
 936 dom forest on the observed parts of the data to predict the missing values. It is particularly  
 937 effective at capturing non-linear interactions without explicit distributional assumptions.

#### 938 Deep Generative Models.

- 939 • **MLP (Multilayer Perceptron)**

940 We use a simple feed-forward neural network with fully connected layers and ReLU activa-  
 941 tions as a deterministic imputation baseline. Given an input vector  $\mathbf{x} \in \mathbb{R}^d$  and a binary  
 942 mask  $\mathbf{m} \in \{0, 1\}^d$  indicating observed entries ( $m_j = 1$  if  $x_j$  is observed, 0 otherwise), we  
 943 first obtain  $\tilde{\mathbf{x}} = \mathbf{x} \odot \mathbf{m} + \mathbf{n} \odot (1 - \mathbf{m})$ , and use the observed mask for input gating:

$$944 \mathbf{h}_0 = \tilde{\mathbf{x}} \odot \mathbf{m}.$$

945 The network  $f_\theta$  takes  $\mathbf{h}_0$  as input and outputs a reconstruction  $\hat{\mathbf{x}} = f_\theta(\mathbf{h}_0)$ . Training is  
 946 performed under weak supervision by minimizing the Mean Squared Error (MSE) *only* on  
 947 observed entries:

$$948 \mathcal{L}_{\text{MLP}} = \|(\hat{\mathbf{x}} - \mathbf{x}) \odot \mathbf{m}\|_2^2,$$

949 so that gradients are propagated only through coordinates with ground-truth observations;  
 950 at test time, the missing entries ( $m_j = 0$ ) are imputed using the corresponding components  
 951 of  $\hat{\mathbf{x}}$ .

- 952 • **VAE (Variational Autoencoder)**

953 Our VAE-based imputer follows the amortized inference framework of Kingma & Welling  
 954 (2013), adapted to incomplete tabular data as in recent work on VAE with missingness (e.g.  
 955 Veldkamp et al. (2025)). Given  $(\mathbf{x}, \mathbf{m})$ , we construct a gated and masked input

$$956 \tilde{\mathbf{x}} = \mathbf{x} \odot \mathbf{m} + \mathbf{n} \odot (1 - \mathbf{m}), \quad \mathbf{h}_0 = \tilde{\mathbf{x}} \odot \mathbf{m},$$

957 and feed the concatenated vector  $[\mathbf{h}_0, \mathbf{1} - \mathbf{m}]$  into the encoder to obtain a Gaussian posterior

$$958 q_\phi(\mathbf{z} \mid \mathbf{x}, \mathbf{m}) = \mathcal{N}(\boldsymbol{\mu}_\phi, \text{diag}(\boldsymbol{\sigma}_\phi^2)).$$

959 A latent sample  $\mathbf{z}$  is drawn via the reparameterization trick and passed through a decoder  
 960  $p_\theta(\mathbf{x} \mid \mathbf{z})$  to produce  $\hat{\mathbf{x}}_\theta(\mathbf{z})$ . The model is trained by maximizing the Evidence Lower  
 961 Bound (ELBO), where the reconstruction term only involves *observed* entries:

$$962 \mathcal{L}_{\text{VAE}} = \underbrace{\|(\hat{\mathbf{x}}_\theta(\mathbf{z}) - \mathbf{x}) \odot \mathbf{m}\|_2^2}_{\text{reconstruction on observed data}} + \underbrace{\text{KL}(q_\phi(\mathbf{z} \mid \mathbf{x}, \mathbf{m}) \parallel p(\mathbf{z}))}_{\text{KL regularization}}.$$

963 At inference time, missing values are imputed by the decoder output  $\hat{\mathbf{x}}_\theta(\mathbf{z})$  at coordinates  
 964 where  $m_j = 0$ .

- 965 • **DAE / mDAE (modified Denoising Autoencoder)**

966 For the autoencoder baseline, we adopt a denoising autoencoder architecture with a modi-  
 967 fication of the loss function proposed in the mDAE Dupuy et al. (2024). Given  $(\mathbf{x}, \mathbf{m})$ , we  
 968 first perform a simple pre-imputation to obtain a complete input  $\tilde{\mathbf{x}}$ , and then apply masking  
 969 noise with rate  $\rho$  *only* on originally observed entries:

$$970 \tilde{\mathbf{x}} = \mathbf{x} \odot \mathbf{m} + \mathbf{n} \odot (1 - \mathbf{m}), \quad \mathbf{c} \sim \text{Ber}(\rho)^d, \quad \tilde{\mathbf{x}}^{(\text{noisy})} = (\tilde{\mathbf{x}} \odot \mathbf{m}) \odot (1 - \mathbf{c} \odot \mathbf{m}).$$

972 The corrupted input  $\tilde{\mathbf{x}}^{(\text{noisy})}$  is fed into an encoder–decoder network  $g_\psi$  that outputs a reconstruction  $\hat{\mathbf{x}} = g_\psi(\tilde{\mathbf{x}}^{(\text{noisy})})$ . Crucially, following the modified-loss idea of mDAE (Dupuy et al., 2024), the reconstruction loss is computed *only on truly observed entries*, and pre-imputed missing values are ignored:  
 973  
 974  
 975  
 976

$$\mathcal{L}_{\text{mDAE}} = \|(\hat{\mathbf{x}} - \mathbf{x}) \odot \mathbf{m}\|_2^2.$$

977 This prevents the autoencoder from overfitting arbitrary pre-imputed values at missing positions while still benefiting from denoising training; at test time, imputations for missing  
 978 entries ( $m_j = 0$ ) are taken from the corresponding components of  $\hat{\mathbf{x}}$ .  
 979  
 980

- **GAIN (Generative Adversarial Imputation Nets) (Yoon et al., 2018)**

981 GAIN adapts the Generative Adversarial Network framework for imputation. The generator  $G$  imputes missing components, while the discriminator  $D$  attempts to distinguish  
 982 between observed and imputed components. A hint mechanism is introduced to provide  $D$   
 983 with partial information about the mask distribution, forcing  $G$  to learn the true underlying  
 984 data distribution. We utilize a hybrid loss function combining adversarial loss with MSE  
 985 for continuous features and cross-entropy for categorical features.  
 986

- **MissDiff (Diffusion Imputation Nets) (Ouyang et al., 2023)**

987 We employ a diffusion probabilistic model specifically adapted for tabular missing data.  
 988 The model is trained to reverse a noise-adding process. During inference (imputation), we  
 989 utilize the *guided sampling* or *conditioning* strategy: at each denoising step  $t$ , the known  
 990 observed values  $\mathbf{x}^{obs}$  ( $\mathbf{x}^{obs} = \mathbf{x} \odot \mathbf{m} + \mathbf{na} \odot (1 - \mathbf{m})$ ) are re-injected into the sample to  
 991 ensure consistency with the ground truth. The model effectively samples  $\mathbf{x}^{imp}$  from the  
 992 conditional distribution  $p(\mathbf{x}^{miss} | \mathbf{x}^{obs})$ .  
 993

994 **Interpretable Models.**  
 995

- **BRCG** (Dash et al., 2018) is an integer program designed to trade classification accuracy for rule simplicity. It uses column generation to search over an exponential number of candidate clauses efficiently.
- **LEN** (Barbiero et al., 2022) is an end-to-end differentiable method for extracting logical explanations from neural networks using First-Order Logic.
- **DR-NET** (Qiao et al., 2021) is a method for learning independent logical rules in disjunctive standard form as an interpretable model for classification.
- **RRL** (Wang et al., 2021) learns interpretable non-fuzzy rules for data representation and classification using a novel training method called Gradient Grafting.

1005 **E PERFORMANCE UNDER DIFFERENT MISSINGNESS MECHANISMS**  
 1006

1007 We compare three general missingness mechanisms for dataset generation:

- **MCR (Missing Completely at Random)**: The probability of being missing is the same for all cases, which is the missingness mechanism in other experiments on our paper.
- **MAR (Missing at Random)**: Missingness depends on observed variables. We can indicate which observed variable to use for missingness; the default is  $X_0$ . Then, we set a higher probability of missing when the dependency variable is 1.
- **MNAR (Missing Not at Random)**: Missingness depends on unobserved variables or the missing values themselves. Take  $X_3$  for example, we set it is more likely to be missing when  $X_3 = 1$  (positive values are harder to observe).

1016 We show an observation ratio = 0.2 and a sample size = 50,000 as a representative case in Table 8.  
 1017 We run 20 random seeds. Since the seeds are different from those used in Tables 23 and 24, the  
 1018 results are slightly different.

1019 Table 8: Comparison of inference accuracy and rule accuracy under different missing mechanisms.  
 1020

	MCAR		MAR		MNAR	
	Imputation Accu.	Rule Accu.	Imputation Accu.	Learned Rules	Imputation Accu.	Rule Accu.
$X_3$	$1.00 \pm 0.00$	1.0	$1.00 \pm 0.00$	1.0000	$1.00 \pm 0.00$	1.0000
$X_4$	$1.00 \pm 0.00$	1.0	$1.00 \pm 0.00$	1.0000	$1.00 \pm 0.00$	1.0000
$X_5$	$0.95 \pm 0.07$	0.6	$0.95 \pm 0.07$	0.6000	$0.93 \pm 0.05$	0.4000

1026 The results show that MAR and MNAR show comparable results to MCAR, which demonstrates  
 1027 our method’s effectiveness across the full spectrum of missing data scenarios.  
 1028

## 1029 F RUNNING TIME AND MEMORY COST ANALYSIS

### 1030 F.1 SYNTHETIC DATASET

1032 While coordinate descent requires different cycle numbers (Table 3), our method demonstrates effi-  
 1033 cient performance on standard CPU configurations. We conducted experiments using an Apple M4  
 1034 chip with 10 cores and 16GB memory, taking observation ratio = 0.2 as an example. Results over  
 1035 20 runs on setting (b) of Figure 3.

1036 Table 9: Running time and memory cost of our model with varying sample sizes. Results over 20  
 1037 seeds on the example (b) of Figure 3.  
 1038

1039 Sample size	1040 2500	1041 5000	1042 10,000	1043 25,000	1044 50,000	1045 100,000
1046 Running time (s)	15.66 $\pm$ 3.48	30.17 $\pm$ 2.12	54.49 $\pm$ 15.98	130.36 $\pm$ 45.80	194.59 $\pm$ 98.53	493.99 $\pm$ 152.81
1047 Memory cost (MB)	64.84 $\pm$ 10.72	71.92 $\pm$ 0.82	78.55 $\pm$ 1.96	95.81 $\pm$ 12.13	126.99 $\pm$ 26.97	175.64 $\pm$ 33.93

1048 Overall, we observe **minimal time and memory costs**. Time complexity scales near-linearly with  
 1049 increasing sample size, while memory requirements remain modest even for large datasets. Process-  
 1050 ing 100,000 samples in under 9 minutes demonstrates strong efficiency for CPU-based execution.

### 1051 F.2 REAL-WORLD DATASET

1052 Table 10: Comparison of running time and memory cost across different methods in SPECT dataset.

1053 Method	1054 Running time (s)	1055 Memory cost (MB)
1056 MLP	0.16 $\pm$ 0.02	158.60 $\pm$ 0.10
1057 LEN	0.20 $\pm$ 0.00	102.78 $\pm$ 0.01
1058 RRL	16.23 $\pm$ 0.01	132.59 $\pm$ 0.01
1059 BRCG	2.65 $\pm$ 0.27	135.11 $\pm$ 0.08
1060 DR-NET	89.01 $\pm$ 0.06	45.93 $\pm$ 0.30
1061 <b>NS-FCN (Ours)</b>	10.34 $\pm$ 0.30	61.42 $\pm$ 1.02

1062 We conducted a comparative analysis of our proposed NS-FCN model against baseline methods,  
 1063 focusing on computational efficiency. We take SPECT dataset as an example. The results in Table  
 1064 demonstrate that NS-FCN achieves a competitive balance between performance and resource  
 1065 consumption. While methods like MLP and LEN offer the fastest execution times, they use higher  
 1066 memory costs. Our NS-FCN, though not the fastest, maintains a considerably minimal memory cost  
 1067 and running time.

## 1068 G ASSESSMENT OF RULE QUALITY

### 1069 G.1 STRUCTURAL STABILITY.

1070 To quantify the structural stability and reliability of the learned rules, we measure the consistency  
 1071 of rule predicates across different random seeds using the Jaccard index. For each rule, we treat  
 1072 the set of instances that satisfy its predicates in a given run as a binary mask, and compute pairwise  
 1073 Jaccard indices between runs obtained under different random seeds and observation probabilities.  
 1074 The **Jaccard index**, defined as the intersection over union of two predicate sets, provides a natural  
 1075 measure of similarity between rule structures learned across independent runs. High mean Jaccard  
 1076 scores (close to 1.0) indicate that the learned rules are structurally stable and robust to stochasticity  
 1077 in training and sampling, whereas lower scores reveal predicates whose semantics are more sensitive  
 1078 to noise or initialization.

1079 **Synthetic Dataset (Figure 3 (b)).** As shown in Table 11, rules  $X_3$  and  $X_4$  achieve perfect Jac-  
 1080 card indices of 1.0 across all observation probabilities, demonstrating complete structural stability.  
 1081 In contrast, the aggregated  $X_5$  rule exhibits more variability (ranging from 0.60 to 0.76), reflecting

1080 the increased complexity of learning disjunctive rule structures. In this way, structural stability—  
 1081 measured via the Jaccard index of predicates across runs—provides a complementary notion of reli-  
 1082 ability that focuses on the consistency of the learned logical structure rather than solely on predictive  
 1083 performance.

1084  
 1085 Table 11: Jaccard index of learned rule predicates on synthetic data under different observation  
 1086 probabilities. Example (b) of Figure 3 with 50,000 samples over 20 seeds.

Obs. Ratio	$X_3$	$X_4$	$X_5$
0.1	$1.0000 \pm 0.0000$	$1.0000 \pm 0.0000$	$0.7572 \pm 0.2526$
0.2	$1.0000 \pm 0.0000$	$1.0000 \pm 0.0000$	$0.5987 \pm 0.2837$
0.3	$1.0000 \pm 0.0000$	$1.0000 \pm 0.0000$	$0.6726 \pm 0.2385$

1087  
 1088  
 1089  
 1090 Table 12: Jaccard Index of learned predicates across different sample sizes on the Birds dataset.  
 1091 Results over 10 seeds.

Sample Size	abnormal_clause1 (ostrich)	abnormal_clause2 (bird $\wedge$ wounded)	can_fly (bird $\wedge$ $\neg$ abnormal_bird)
100	$0.8000 \pm 0.2449$	$0.5000 \pm 0.3162$	$0.5000 \pm 0.3162$
500	$0.8000 \pm 0.2449$	$0.8000 \pm 0.2449$	$0.7000 \pm 0.2449$
1000	$0.8000 \pm 0.2449$	$0.6000 \pm 0.3000$	$0.6000 \pm 0.3000$
1500	$0.8187 \pm 0.2404$	$0.6868 \pm 0.3024$	$0.7967 \pm 0.2670$
2000	$0.8000 \pm 0.2449$	$0.6000 \pm 0.3000$	$0.6000 \pm 0.3000$

1092  
 1093  
 1094 **Birds Dataset.** We analyze the consistency of learned rule structures in Birds Dataset (Figure 5).  
 1095 Table 12 presents the Jaccard indices across all pairwise comparisons between seeds for different  
 1096 sample sizes, where *abnormal\_clause1* and *abnormal\_clause2* correspond to the two conjunctive  
 1097 clauses in the disjunctive rule for *abnormal\_bird*:  $abnormal\_bird \leftarrow ostrich \vee (bird \wedge wounded)$ .

1098 The results demonstrate that, with the exception of  $n = 100$  where the sample size is insufficient, the  
 1099 model achieves good consistency (Jaccard index  $> 0.60$ ) across all rules and sample sizes. Overall,  
 1100  $n = 1500$  yields the best consistency, with *abnormal\_clause1* reaching 0.8187 and *can\_fly* reaching  
 1101 0.7967, indicating that this sample size provides an optimal balance between data availability and  
 1102 model stability.

1103  
 1104 Table 13: Structural stability of learned prediction rules on the Heart Disease dataset.

Metric	Value
<b>Mean Pairwise Jaccard Index</b>	$0.4151 \pm 0.0994$
<b>Most Frequently Selected Features</b>	
<i>restecg_1.0</i> (ST-T wave abnormality)	9/10 runs
<i>thal_3.0</i> (normal thalassemia)	8/10 runs
<i>ca_3.0</i> (3 major vessels colored)	8/10 runs
<i>thalach</i> (maximum heart rate achieved)	7/10 runs

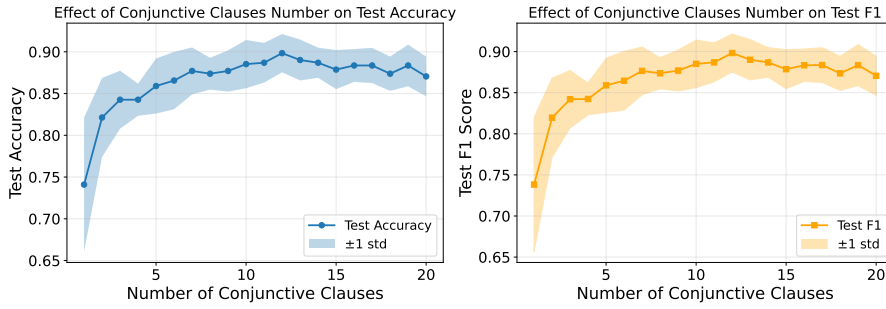
1105  
 1106  
 1107 **Heart Disease dataset.** For this real-world dataset, where ground-truth rules are unknown, we  
 1108 evaluate structural stability by computing the Jaccard index of selected features across all predic-  
 1109 tion rules learned under different random seeds. Table 13 shows that the model achieves moderate  
 1110 consistency (Jaccard index  $0.4151 \pm 0.0994$ ), indicating that while different seeds may select vary-  
 1111 ing feature combinations, there is substantial overlap in the most important features. The most  
 1112 frequently selected features include *restecg\_1.0* (ST-T wave abnormality on resting electrocardiogram),  
 1113 *thal\_3.0* (normal thalassemia, a blood disorder), *ca\_3.0* (three major vessels colored by fluoroscopy,  
 1114 indicating severe coronary artery disease), and *thalach* (maximum heart rate achieved during  
 1115 exercise). These features align with established clinical risk factors for heart disease, suggesting that the  
 1116 model successfully identifies medically relevant features despite the lack of explicit rule supervision.

1134  
1135 

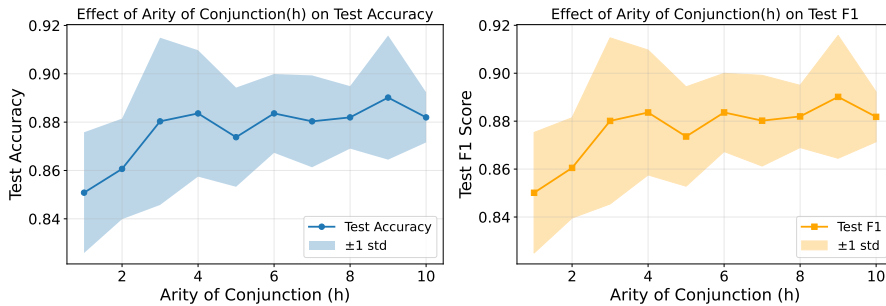
## G.2 RULE LENGTH ANALYSIS

1136 To understand the sensitivity of our framework to the rule structure hyperparameters, we conduct  
 1137 ablation studies on the Heart Disease dataset, systematically varying the arity of conjunction ( $h$ ) and  
 1138 the number of conjunctive clauses ( $R_k$ ).

1139 We find that both  $h$  and  $R_k$  show optimal performance in a wide range. For instance,  $h \in [3, 9]$  and  
 1140  $R_k \in [5, 20]$ , showing that except for very small  $h$  and  $R_k$ , our model is able to capture the logic  
 1141 structure within the dataset. Besides, the number of disjunctive clauses is more critical than the arity  
 1142 of individual conjunctions for this dataset. This aligns with the intuition that complex real-world  
 1143 decision boundaries often require multiple alternative rules rather than highly complex single rules.



1144  
1145  
1146  
1147  
1148  
1149  
1150  
1151  
1152  
1153  
1154  
1155 Figure 6: Classification accuracy for heart disease risk under the effect of the number of conjunction  
 1156 arity ( $h$ ). Results are over 10 seeds.



1157  
1158  
1159  
1160  
1161  
1162  
1163  
1164  
1165  
1166  
1167  
1168  
1169  
1170  
1171  
1172  
1173  
1174  
1175  
1176  
1177  
1178  
1179  
1180  
1181  
1182  
1183  
1184  
1185  
1186  
1187  
1188  
1189  
1190  
1191  
1192  
1193  
1194  
1195  
1196  
1197  
1198  
1199  
1200  
1201  
1202  
1203  
1204  
1205  
1206  
1207  
1208  
1209  
1210  
1211  
1212  
1213  
1214  
1215  
1216  
1217  
1218  
1219  
1220  
1221  
1222  
1223  
1224  
1225  
1226  
1227  
1228  
1229  
1230  
1231  
1232  
1233  
1234  
1235  
1236  
1237  
1238  
1239  
1240  
1241  
1242  
1243  
1244  
1245  
1246  
1247  
1248  
1249  
1250  
1251  
1252  
1253  
1254  
1255  
1256  
1257  
1258  
1259  
1260  
1261  
1262  
1263  
1264  
1265  
1266  
1267  
1268  
1269  
1270  
1271  
1272  
1273  
1274  
1275  
1276  
1277  
1278  
1279  
1280  
1281  
1282  
1283  
1284  
1285  
1286  
1287  
1288  
1289  
1290  
1291  
1292  
1293  
1294  
1295  
1296  
1297  
1298  
1299  
1300  
1301  
1302  
1303  
1304  
1305  
1306  
1307  
1308  
1309  
1310  
1311  
1312  
1313  
1314  
1315  
1316  
1317  
1318  
1319  
1320  
1321  
1322  
1323  
1324  
1325  
1326  
1327  
1328  
1329  
1330  
1331  
1332  
1333  
1334  
1335  
1336  
1337  
1338  
1339  
1340  
1341  
1342  
1343  
1344  
1345  
1346  
1347  
1348  
1349  
1350  
1351  
1352  
1353  
1354  
1355  
1356  
1357  
1358  
1359  
1360  
1361  
1362  
1363  
1364  
1365  
1366  
1367  
1368  
1369  
1370  
1371  
1372  
1373  
1374  
1375  
1376  
1377  
1378  
1379  
1380  
1381  
1382  
1383  
1384  
1385  
1386  
1387  
1388  
1389  
1390  
1391  
1392  
1393  
1394  
1395  
1396  
1397  
1398  
1399  
1400  
1401  
1402  
1403  
1404  
1405  
1406  
1407  
1408  
1409  
1410  
1411  
1412  
1413  
1414  
1415  
1416  
1417  
1418  
1419  
1420  
1421  
1422  
1423  
1424  
1425  
1426  
1427  
1428  
1429  
1430  
1431  
1432  
1433  
1434  
1435  
1436  
1437  
1438  
1439  
1440  
1441  
1442  
1443  
1444  
1445  
1446  
1447  
1448  
1449  
1450  
1451  
1452  
1453  
1454  
1455  
1456  
1457  
1458  
1459  
1460  
1461  
1462  
1463  
1464  
1465  
1466  
1467  
1468  
1469  
1470  
1471  
1472  
1473  
1474  
1475  
1476  
1477  
1478  
1479  
1480  
1481  
1482  
1483  
1484  
1485  
1486  
1487  
1488  
1489  
1490  
1491  
1492  
1493  
1494  
1495  
1496  
1497  
1498  
1499  
1500  
1501  
1502  
1503  
1504  
1505  
1506  
1507  
1508  
1509  
1510  
1511  
1512  
1513  
1514  
1515  
1516  
1517  
1518  
1519  
1520  
1521  
1522  
1523  
1524  
1525  
1526  
1527  
1528  
1529  
1530  
1531  
1532  
1533  
1534  
1535  
1536  
1537  
1538  
1539  
1540  
1541  
1542  
1543  
1544  
1545  
1546  
1547  
1548  
1549  
1550  
1551  
1552  
1553  
1554  
1555  
1556  
1557  
1558  
1559  
1560  
1561  
1562  
1563  
1564  
1565  
1566  
1567  
1568  
1569  
1570  
1571  
1572  
1573  
1574  
1575  
1576  
1577  
1578  
1579  
1580  
1581  
1582  
1583  
1584  
1585  
1586  
1587  
1588  
1589  
1590  
1591  
1592  
1593  
1594  
1595  
1596  
1597  
1598  
1599  
1600  
1601  
1602  
1603  
1604  
1605  
1606  
1607  
1608  
1609  
1610  
1611  
1612  
1613  
1614  
1615  
1616  
1617  
1618  
1619  
1620  
1621  
1622  
1623  
1624  
1625  
1626  
1627  
1628  
1629  
1630  
1631  
1632  
1633  
1634  
1635  
1636  
1637  
1638  
1639  
1640  
1641  
1642  
1643  
1644  
1645  
1646  
1647  
1648  
1649  
1650  
1651  
1652  
1653  
1654  
1655  
1656  
1657  
1658  
1659  
1660  
1661  
1662  
1663  
1664  
1665  
1666  
1667  
1668  
1669  
1670  
1671  
1672  
1673  
1674  
1675  
1676  
1677  
1678  
1679  
1680  
1681  
1682  
1683  
1684  
1685  
1686  
1687  
1688  
1689  
1690  
1691  
1692  
1693  
1694  
1695  
1696  
1697  
1698  
1699  
1700  
1701  
1702  
1703  
1704  
1705  
1706  
1707  
1708  
1709  
1710  
1711  
1712  
1713  
1714  
1715  
1716  
1717  
1718  
1719  
1720  
1721  
1722  
1723  
1724  
1725  
1726  
1727  
1728  
1729  
1730  
1731  
1732  
1733  
1734  
1735  
1736  
1737  
1738  
1739  
1740  
1741  
1742  
1743  
1744  
1745  
1746  
1747  
1748  
1749  
1750  
1751  
1752  
1753  
1754  
1755  
1756  
1757  
1758  
1759  
1760  
1761  
1762  
1763  
1764  
1765  
1766  
1767  
1768  
1769  
1770  
1771  
1772  
1773  
1774  
1775  
1776  
1777  
1778  
1779  
1780  
1781  
1782  
1783  
1784  
1785  
1786  
1787  
1788  
1789  
1790  
1791  
1792  
1793  
1794  
1795  
1796  
1797  
1798  
1799  
1800  
1801  
1802  
1803  
1804  
1805  
1806  
1807  
1808  
1809  
1810  
1811  
1812  
1813  
1814  
1815  
1816  
1817  
1818  
1819  
1820  
1821  
1822  
1823  
1824  
1825  
1826  
1827  
1828  
1829  
1830  
1831  
1832  
1833  
1834  
1835  
1836  
1837  
1838  
1839  
1840  
1841  
1842  
1843  
1844  
1845  
1846  
1847  
1848  
1849  
1850  
1851  
1852  
1853  
1854  
1855  
1856  
1857  
1858  
1859  
1860  
1861  
1862  
1863  
1864  
1865  
1866  
1867  
1868  
1869  
1870  
1871  
1872  
1873  
1874  
1875  
1876  
1877  
1878  
1879  
1880  
1881  
1882  
1883  
1884  
1885  
1886  
1887  
1888  
1889  
1890  
1891  
1892  
1893  
1894  
1895  
1896  
1897  
1898  
1899  
1900  
1901  
1902  
1903  
1904  
1905  
1906  
1907  
1908  
1909  
1910  
1911  
1912  
1913  
1914  
1915  
1916  
1917  
1918  
1919  
1920  
1921  
1922  
1923  
1924  
1925  
1926  
1927  
1928  
1929  
1930  
1931  
1932  
1933  
1934  
1935  
1936  
1937  
1938  
1939  
1940  
1941  
1942  
1943  
1944  
1945  
1946  
1947  
1948  
1949  
1950  
1951  
1952  
1953  
1954  
1955  
1956  
1957  
1958  
1959  
1960  
1961  
1962  
1963  
1964  
1965  
1966  
1967  
1968  
1969  
1970  
1971  
1972  
1973  
1974  
1975  
1976  
1977  
1978  
1979  
1980  
1981  
1982  
1983  
1984  
1985  
1986  
1987  
1988  
1989  
1990  
1991  
1992  
1993  
1994  
1995  
1996  
1997  
1998  
1999  
2000  
2001  
2002  
2003  
2004  
2005  
2006  
2007  
2008  
2009  
2010  
2011  
2012  
2013  
2014  
2015  
2016  
2017  
2018  
2019  
2020  
2021  
2022  
2023  
2024  
2025  
2026  
2027  
2028  
2029  
2030  
2031  
2032  
2033  
2034  
2035  
2036  
2037  
2038  
2039  
2040  
2041  
2042  
2043  
2044  
2045  
2046  
2047  
2048  
2049  
2050  
2051  
2052  
2053  
2054  
2055  
2056  
2057  
2058  
2059  
2060  
2061  
2062  
2063  
2064  
2065  
2066  
2067  
2068  
2069  
2070  
2071  
2072  
2073  
2074  
2075  
2076  
2077  
2078  
2079  
2080  
2081  
2082  
2083  
2084  
2085  
2086  
2087  
2088  
2089  
2090  
2091  
2092  
2093  
2094  
2095  
2096  
2097  
2098  
2099  
2100  
2101  
2102  
2103  
2104  
2105  
2106  
2107  
2108  
2109  
2110  
2111  
2112  
2113  
2114  
2115  
2116  
2117  
2118  
2119  
2120  
2121  
2122  
2123  
2124  
2125  
2126  
2127  
2128  
2129  
2130  
2131  
2132  
2133  
2134  
2135  
2136  
2137  
2138  
2139  
2140  
2141  
2142  
2143  
2144  
2145  
2146  
2147  
2148  
2149  
2150  
2151  
2152  
2153  
2154  
2155  
2156  
2157  
2158  
2159  
2160  
2161  
2162  
2163  
2164  
2165  
2166  
2167  
2168  
2169  
2170  
2171  
2172  
2173  
2174  
2175  
2176  
2177  
2178  
2179  
2180  
2181  
2182  
2183  
2184  
2185  
2186  
2187  
2188  
2189  
2190  
2191  
2192  
2193  
2194  
2195  
2196  
2197  
2198  
2199  
2200  
2201  
2202  
2203  
2204  
2205  
2206  
2207  
2208  
2209  
2210  
2211  
2212  
2213  
2214  
2215  
2216  
2217  
2218  
2219  
2220  
2221  
2222  
2223  
2224  
2225  
2226  
2227  
2228  
2229  
22210  
22211  
22212  
22213  
22214  
22215  
22216  
22217  
22218  
22219  
22220  
22221  
22222  
22223  
22224  
22225  
22226  
22227  
22228  
22229  
222210  
222211  
222212  
222213  
222214  
222215  
222216  
222217  
222218  
222219  
222220  
222221  
222222  
222223  
222224  
222225  
222226  
222227  
222228  
222229  
2222210  
2222211  
2222212  
2222213  
2222214  
2222215  
2222216  
2222217  
2222218  
2222219  
2222220  
2222221  
2222222  
2222223  
2222224  
2222225  
2222226  
2222227  
2222228  
2222229  
22222210  
22222211  
22222212  
22222213  
22222214  
22222215  
22222216  
22222217  
22222218  
22222219  
22222220  
22222221  
22222222  
22222223  
22222224  
22222225  
22222226  
22222227  
22222228  
22222229  
222222210  
222222211  
222222212  
222222213  
222222214  
222222215  
222222216  
222222217  
222222218  
222222219  
222222220  
222222221  
222222222  
222222223  
222222224  
222222225  
222222226  
222222227  
222222228  
222222229  
2222222210  
2222222211  
2222222212  
2222222213  
2222222214  
2222222215  
2222222216  
2222222217  
2222222218  
2222222219  
2222222220  
2222222221  
2222222222  
2222222223  
2222222224  
2222222225  
2222222226  
2222222227  
2222222228  
2222222229  
22222222210  
22222222211  
22222222212  
22222222213  
22222222214  
22222222215  
22222222216  
22222222217  
22222222218  
22222222219  
22222222220  
22222222221  
22222222222  
22222222223  
22222222224  
22222222225  
22222222226  
22222222227  
22222222228  
22222222229  
222222222210  
222222222211  
222222222212  
222222222213  
222222222214  
222222222215  
222222222216  
222222222217  
222222222218  
222222222219  
222222222220  
222222222221  
222222222222  
222222222223  
222222222224  
222222222225  
222222222226  
222222222227  
222222222228  
222222222229  
2222222222210  
2222222222211  
2222222222212  
2222222222213  
2222222222214  
2222222222215  
2222222222216  
2222222222217  
2222222222218  
2222222222219  
2222222222220  
2222222222221  
2222222222222  
2222222222223  
2222222222224  
2222222222225  
2222222222226  
2222222222227  
2222222222228  
2222222222229  
22222222222210  
22222222222211  
22222222222212  
22222222222213  
22222222222214  
22222222222215  
22222222222216  
22222222222217  
22222222222218  
22222222222219  
22222222222220  
22222222222221  
22222222222222  
22222222222223  
22222222222224  
22222222222225  
22222222222226  
22222222222227  
22222222222228  
22222222222229  
222222222222210  
222222222222211  
222222222222212  
222222222222213  
222222222222214  
222222222222215  
222222222222216  
222222222222217  
222222222222218  
222222222222219  
222222222222220  
222222222222221  
222222222222222  
222222222222223  
222222222222224  
222222222222225  
222222222222226  
222222222222227  
222222222222228  
222222222222229  
2222222222222210  
2222222222222211  
2222222222222212  
2222222222222213  
2222222222222214  
2222222222222215  
2222222222222216  
2222222222222217  
2222222222222218  
2222222222222219  
2222222222222220  
2222222222222221  
2222222222222222  
2222222222222223  
2222222222222224  
2222222222222225  
2222222222222226  
2222222222222227  
2222222222222228  
2222222222222229  
22222222222222210  
22222222222222211  
22222222222222212  
22222222222222213  
22222222222222214  
22222222222222215  
22222222222222216  
22222222222222217  
22222222222222218  
22222222222222219  
22222222222222220  
22222222222222221  
22222222222222222  
22222222222222223  
22222222222222224  
22222222222222225  
22222222222222226  
22222222222222227  
22222222222222228  
22222222222222229  
222222222222222210  
222222222222222211  
222222222222222212  
222222222222222213  
222222222222222214  
222222222222222215  
222222222222222216  
222222222222222217  
222222222222222218  
222222222222222219  
222222222222222220  
222222222222222221  
222222222222222222  
222222222222222223  
222222222222222224  
222222222222222225  
222222222222222226  
222222222222222227  
222222222222222228  
222222222222222229  
2222222222222222210  
2222222222222222211  
2222222222222222212  
2222222222222222213  
2222222222222222214  
2222222222222222215  
2222222222222222216  
2222222222222222217  
2222222222222222218  
2222222222222222219  
2222222222222222220  
22222222

1188 Table 14: Imputation accuracy for latent predicates  $X_3, X_4, X_5$  under different softmin temperatures  
 1189 (with fixed  $\beta = 10$  over 20 random seeds).

1190

$\tau$ in Equation 4	Imputation Acc. X3	Imputation Acc. X4	Imputation Acc. X5
0.01	1.000 $\pm$ 0.000	1.000 $\pm$ 0.000	0.965 $\pm$ 0.063
0.02	1.000 $\pm$ 0.000	1.000 $\pm$ 0.000	0.987 $\pm$ 0.034
0.05	1.000 $\pm$ 0.000	1.000 $\pm$ 0.000	0.939 $\pm$ 0.061
0.10	1.000 $\pm$ 0.000	1.000 $\pm$ 0.000	0.958 $\pm$ 0.076
0.20	1.000 $\pm$ 0.000	1.000 $\pm$ 0.000	1.000 $\pm$ 0.000
0.50	1.000 $\pm$ 0.000	1.000 $\pm$ 0.000	0.858 $\pm$ 0.038
1.00	0.928 $\pm$ 0.122	0.892 $\pm$ 0.134	0.776 $\pm$ 0.027
2.00	0.751 $\pm$ 0.002	0.839 $\pm$ 0.157	0.786 $\pm$ 0.008
5.00	0.769 $\pm$ 0.111	0.750 $\pm$ 0.003	0.772 $\pm$ 0.083
10.00	0.752 $\pm$ 0.003	0.770 $\pm$ 0.111	0.802 $\pm$ 0.064
20.00	0.697 $\pm$ 0.098	0.733 $\pm$ 0.046	0.799 $\pm$ 0.064
50.00	0.733 $\pm$ 0.049	0.733 $\pm$ 0.046	0.798 $\pm$ 0.077
100.00	0.750 $\pm$ 0.004	0.698 $\pm$ 0.064	0.803 $\pm$ 0.069

1205 Table 15: Imputation accuracy for latent predicates  $X_3, X_4, X_5$  under different constant temperature  
 1206 values  $\beta$  (with fixed  $\tau = 0.1$  over 20 random seeds).

1207

$\beta$ of Equation 5	Imputation Acc. X3	Imputation Acc. X4	Imputation Acc. X5
0.1	1.000 $\pm$ 0.000	1.000 $\pm$ 0.000	0.218 $\pm$ 0.002
0.2	1.000 $\pm$ 0.000	1.000 $\pm$ 0.000	0.218 $\pm$ 0.002
0.5	1.000 $\pm$ 0.000	1.000 $\pm$ 0.000	0.218 $\pm$ 0.002
1	1.000 $\pm$ 0.000	1.000 $\pm$ 0.000	0.217 $\pm$ 0.002
2	1.000 $\pm$ 0.000	1.000 $\pm$ 0.000	0.870 $\pm$ 0.117
3	1.000 $\pm$ 0.000	1.000 $\pm$ 0.000	0.942 $\pm$ 0.056
4	1.000 $\pm$ 0.000	1.000 $\pm$ 0.000	0.866 $\pm$ 0.057
5	0.965 $\pm$ 0.093	1.000 $\pm$ 0.000	0.894 $\pm$ 0.056
10	0.965 $\pm$ 0.093	1.000 $\pm$ 0.000	0.915 $\pm$ 0.040
15	0.965 $\pm$ 0.092	1.000 $\pm$ 0.000	0.899 $\pm$ 0.072
20	0.966 $\pm$ 0.091	1.000 $\pm$ 0.000	0.928 $\pm$ 0.057
25	0.965 $\pm$ 0.092	1.000 $\pm$ 0.000	0.886 $\pm$ 0.060
30	1.000 $\pm$ 0.000	1.000 $\pm$ 0.000	0.899 $\pm$ 0.088
35	0.965 $\pm$ 0.093	1.000 $\pm$ 0.000	0.880 $\pm$ 0.076
40	1.000 $\pm$ 0.000	1.000 $\pm$ 0.000	0.889 $\pm$ 0.075
45	0.964 $\pm$ 0.094	0.965 $\pm$ 0.093	0.909 $\pm$ 0.051
50	1.000 $\pm$ 0.000	1.000 $\pm$ 0.000	0.917 $\pm$ 0.064
100	0.965 $\pm$ 0.094	1.000 $\pm$ 0.000	0.916 $\pm$ 0.064
200	1.000 $\pm$ 0.000	1.000 $\pm$ 0.000	0.908 $\pm$ 0.070

1227

1228 **Conclusion.** Our framework does not rely on carefully hyperparameter tuning. A moderate  
 1229 to large  $\beta$  for Soft-OR and a small  $\tau$  for Soft-AND consistently yield optimal results. Thus, we  
 1230 use  $\tau = 0.1$  and  $\beta = 10$  as temperature parameters for all our experiments. Furthermore, complex  
 1231 scheduling strategies like cosine annealing can be employed if constant temperature are not good  
 1232 enough.

1233

## I SENSITIVITY ANALYSIS WITH LABEL NOISE AND MISSING RATIO

1234

### I.1 ROBUSTNESS ANALYSIS WITH LABEL NOISE

1235

To assess the robustness of our framework against data inconsistencies and imperfect logical dependencies, we conducted experiments by injecting label noise into the latent predicates.

1236

1237 Specifically, we first generate the ground-truth latent predicates  $X_3, X_4, X_5$  following the perfect  
 1238 logical rules (e.g.,  $X_3 = X_0 \wedge X_1$ ). Then, we introduce stochasticity by flipping the binary labels  
 1239 of these latent predicates with a probability  $p_{noise} \in \{0.0, 0.1, 0.2, 0.3, 0.4, 0.5\}$ . This setup simu-  
 1240 lates real-world scenarios where logical rules may have exceptions or where the observed data  
 1241 contains errors, directly challenging the model’s ability to distill consistent symbolic rules from

1242  
 1243 **noisy supervision.** Tables 16 and 17 present the learned rule structures and their corresponding im-  
 1244 putation accuracies under varying noise ratios. We use Figure 3 (b) as the representative example  
 1245 with an observation ratio of 0.3 and sample sizes of 20,000.

1246 In the noise-free setting ( $p_{noise} = 0.0$ ), our model perfectly recovers the ground-truth rules for  
 1247 the simpler conjunctive predicates  $X_3$  and  $X_4$  (with rule accuracy 1.00), achieving perfect imputa-  
 1248 tion accuracy (1.000). For the more complex disjunctive rule  $X_5$ , the model achieves a rule accu-  
 1249 racy of 0.50 and an imputation accuracy of 0.955 after fine-tuning, indicating that while the exact  
 1250 ground-truth structure is harder to isolate, the learned approximations maintain strong predictive  
 1251 performance.

1252 Remarkably, the model demonstrates strong robustness at low-to-moderate noise levels ( $p_{noise} \leq$   
 1253 0.3). At  $p_{noise} = 0.1$  and 0.2, the ground-truth rules (underlined in the table) for  $X_3$  and  $X_4$  are  
 1254 perfectly recovered (rule accuracy 1.00) with near-perfect imputation accuracies; for the complex  
 1255 multi-hop rules of  $X_5$ , the ground-truth rules frequently emerge as the dominant learned structures  
 1256 (with rule accuracy above 0.5). Even at  $p_{noise} = 0.3$ , the model maintains high rule accuracy (0.85)  
 1257 for both  $X_3$  and  $X_4$ , with imputation accuracies above 0.95; for  $X_5$ , the rule accuracy decreases to  
 1258 0.2 at  $p_{noise} = 0.3$ , but the imputation accuracy remains at 0.828, suggesting that **the model learns**  
 1259 **valid approximations (e.g., capturing one correct disjunctive branch) that preserve predictive**  
 1260 **power.**

1261 As noise increases beyond 0.3, the performance degrades more significantly. At  $p_{noise} = 0.4$ , rule  
 1262 accuracies drop to 0.85 and 0.6 for  $X_3$  and  $X_4$  respectively, while  $X_5$  fails to recover the correct  
 1263 structure (rule accuracy 0.00). At  $p_{noise} = 0.5$ , the model struggles to learn meaningful rules, with  
 1264 rule accuracies in [0.0, 0.1] for all predicates. However, the imputation accuracies remain above  
 1265 0.70 even at these high noise levels, indicating that the learned approximations, while not perfectly  
 1266 matching the ground-truth rules, still provide useful predictive signals.

1267 The imputation accuracy degrades gracefully as noise increases, rather than collapsing abruptly,  
 1268 indicating that **the soft-logic relaxation effectively prevents the model from overfitting to noise**,  
 1269 allowing it to capture the dominant logical signals within the data. The fine-tuning step for  $X_5$   
 1270 consistently improves imputation accuracy across all noise levels, demonstrating the effectiveness  
 1271 of the iterative refinement process.

1272 Table 16: Impact of label noise on rule learning and missing value imputation performance. Results  
 1273 are over 20 random seeds.

1274 Noise Ratio	1275 Avg. Imputation Accu. (Before Fine-tune)	1276 Avg. Imputation Accu. (After Fine-tune)	1277 Train Loss (Before Fine-tune)	1278 Train Loss (After Fine-tune)
0.0	$X_3 : 1.000 \pm 0.000$	/	$X_3 : 0.001 \pm 0.000$	/
	$X_4 : 1.000 \pm 0.000$	/	$X_4 : 0.001 \pm 0.000$	/
	$X_5 : 0.907 \pm 0.050$	$X_5 : 0.955 \pm 0.049$	$X_5 : 0.089 \pm 0.035$	$X_5 : 0.067 \pm 0.031$
0.1	$X_3 : 1.000 \pm 0.000$	/	$X_3 : 0.098 \pm 0.003$	/
	$X_4 : 1.000 \pm 0.000$	/	$X_4 : 0.099 \pm 0.004$	/
	$X_5 : 0.948 \pm 0.042$	$X_5 : 0.946 \pm 0.038$	$X_5 : 0.168 \pm 0.026$	$X_5 : 0.123 \pm 0.021$
0.2	$X_3 : 0.975 \pm 0.076$	/	$X_3 : 0.193 \pm 0.005$	/
	$X_4 : 0.987 \pm 0.057$	/	$X_4 : 0.193 \pm 0.007$	/
	$X_5 : 0.894 \pm 0.050$	$X_5 : 0.902 \pm 0.046$	$X_5 : 0.260 \pm 0.008$	$X_5 : 0.204 \pm 0.012$
0.3	$X_3 : 0.950 \pm 0.103$	/	$X_3 : 0.282 \pm 0.006$	/
	$X_4 : 0.987 \pm 0.056$	/	$X_4 : 0.282 \pm 0.008$	/
	$X_5 : 0.822 \pm 0.046$	$X_5 : 0.824 \pm 0.066$	$X_5 : 0.320 \pm 0.006$	$X_5 : 0.266 \pm 0.006$
0.4	$X_3 : 0.863 \pm 0.127$	/	$X_3 : 0.360 \pm 0.009$	/
	$X_4 : 0.862 \pm 0.128$	/	$X_4 : 0.357 \pm 0.008$	/
	$X_5 : 0.792 \pm 0.078$	$X_5 : 0.786 \pm 0.065$	$X_5 : 0.370 \pm 0.006$	$X_5 : 0.311 \pm 0.006$
0.5	$X_3 : 0.745 \pm 0.085$	/	$X_3 : 0.418 \pm 0.007$	/
	$X_4 : 0.725 \pm 0.077$	/	$X_4 : 0.421 \pm 0.007$	/
	$X_5 : 0.761 \pm 0.057$	$X_5 : 0.767 \pm 0.072$	$X_5 : 0.421 \pm 0.007$	$X_5 : 0.349 \pm 0.007$

1291

1292

1293

1294

## I.2 MISSING RATIO

1295

In three synthetic datasets, we have varied the missing ratio in {0.7, 0.8, 0.9} in the above results.

1296 Table 17: Learned rule structures under label noise. Ground truth rules are indicated with underlines.  
1297 Results are over 20 random seeds.  
1298

1299	1300	1301	1302	1303	1304	1305	1306	1307	1308	1309	1310	1311	Rule Accu.
	0.0	$X_3 : \underline{X_0 \wedge X_1}$ $X_4 : \underline{X_2 \wedge X_7}$ $X_5 : (\underline{X_0 \wedge X_4}) \vee (X_3 \wedge X_6), (X_3 \wedge X_4) \vee (X_3 \wedge X_6), (X_0 \wedge X_4) \vee (X_0 \wedge X_4), (X_0 \wedge X_4) \vee (X_1 \wedge X_6), (X_1 \wedge X_3) \vee (X_3 \wedge X_6)$											$X_3 : 1.00$ $X_4 : 1.00$ $X_5 : 0.50$
	0.1	$X_3 : \underline{X_0 \wedge X_1}$ $X_4 : \underline{X_2 \wedge X_7}$ $X_5 : (\underline{X_0 \wedge X_4}) \vee (X_3 \wedge X_6), (X_3 \wedge X_4) \vee (X_3 \wedge X_6), (X_0 \wedge X_4) \vee (X_0 \wedge X_4), (X_0 \wedge X_4) \vee (X_1 \wedge X_6), (X_1 \wedge X_3) \vee (X_3 \wedge X_6)$											$X_3 : 1.00$ $X_4 : 1.00$ $X_5 : 0.55$
	0.2	$X_3 : \underline{X_0 \wedge X_1}$ $X_4 : \underline{X_2 \wedge X_7}$ $X_5 : (\underline{X_0 \wedge X_4}) \vee (X_3 \wedge X_6), (X_3 \wedge X_4) \vee (X_3 \wedge X_6), (X_0 \wedge X_4) \vee (X_0 \wedge X_4), (X_0 \wedge X_4) \vee (X_2 \wedge X_3), (X_0 \wedge X_2) \vee (X_3 \wedge X_6)$											$X_3 : 1.00$ $X_4 : 1.00$ $X_5 : 0.60$
	0.3	$X_3 : X_0 \wedge X_1, X_1 \wedge X_2, X_1 \wedge X_1, X_1 \wedge X_7$ $X_4 : \underline{X_2 \wedge X_7}, X_2 \wedge X_6, X_2 \wedge X_2$ $X_5 : (\underline{X_0 \wedge X_4}) \vee (X_3 \wedge X_6), (X_0 \wedge X_7) \vee (X_3 \wedge X_6), (X_0 \wedge X_3) \vee (X_0 \wedge X_1), (X_3 \wedge X_6) \vee (X_1 \wedge X_7), (X_0 \wedge X_1) \vee (X_0 \wedge X_6)$											$X_3 : 0.85$ $X_4 : 0.85$ $X_5 : 0.20$
	0.4	$X_3 : X_0 \wedge X_1, X_1 \wedge X_1, X_1 \wedge X_2, X_0 \wedge X_6, X_0 \wedge X_0$ $X_4 : \underline{X_2 \wedge X_7}, X_7 \wedge X_7, X_0 \wedge X_2, X_0 \wedge X_0, X_2 \wedge X_6$ $X_5 : (\underline{X_0 \wedge X_2}) \vee (X_4 \wedge X_6), (X_0 \wedge X_6) \vee (X_3 \wedge X_3), (X_0 \wedge X_2) \vee (X_2 \wedge X_3), (X_0 \wedge X_6) \vee (X_1 \wedge X_7), (X_1 \wedge X_4) \vee (X_4 \wedge X_4)$											$X_3 : 0.60$ $X_4 : 0.60$ $X_5 : 0.00$
	0.5	$X_3 : X_1 \wedge X_7, X_2 \wedge X_2, X_6 \wedge X_6, X_0 \wedge X_2, X_0 \wedge X_1$ $X_4 : X_6 \wedge X_6, X_0 \wedge X_6, X_0 \wedge X_7, X_6 \wedge X_7, X_1 \wedge X_2$ $X_5 : (X_0 \wedge X_3) \vee (X_1 \wedge X_6), (X_0 \wedge X_2) \vee (X_2 \wedge X_7), (X_0 \wedge X_0) \vee (X_2 \wedge X_7), (X_0 \wedge X_3) \vee (X_4 \wedge X_7), (X_2 \wedge X_7) \vee (X_0 \wedge X_7)$											$X_3 : 0.10$ $X_4 : 0.05$ $X_5 : 0.00$

1312 In real-world datasets, to assess the model’s robustness under different levels of data scarcity, we  
1313 evaluated its performance on the SPECT and Heart Disease dataset while varying the observation  
1314 ratio from 0.3 to 0.9 (i.e. missing ratio from 0.1 to 0.7).

1315 As shown in Tables 18 and 19, the model’s accuracy remains acceptable and improves consistently  
1316 as more data becomes available. Notably, in SPECT, even with only 30% of the data observed (a  
1317 70% missing ratio), the model maintains a high F1 score of 0.751, demonstrating its capability to  
1318 learn meaningful diagnostic rules from highly incomplete datasets.

1319 For the Birds Dataset, we fix the observation ratio as 0.1 (i.e. 90% missingness) and show results  
1320 over different number of training samples. Results in Table 20 show that a few hundred samples are  
1321 sufficient for the model to converge to the correct logical truth.

1322 Table 18: Performance on the SPECT dataset with varying observation ratios.  
1323

1324	1325	Observation Ratio	1326	1327	1328	1329	Imputation Acc.	1326	1327	1328	1329	Diagnosis Acc.	1326	1327	1328	1329	Diagnosis F1
		0.3					0.501					0.679				0.751	
		0.5					0.630					0.765				0.808	
		0.7					0.763					0.920				0.958	
		0.9					0.791					0.929				0.960	

1331 Table 19: Imputation accuracy for Heart Disease under different observation ratios.  
1332

1333	1334	Observation Ratio	1335	1336	1337	1338	Overall	1335	1336	1337	1338	trestbps	1335	1336	1337	1338	thalach	1335	1336	1337	1338	oldpeak
		0.3					0.6444					0.7129					0.6304				0.7393	0.4950
		0.5					0.7434					0.8053					0.7558				0.7954	0.6172
		0.7					0.8432					0.8647					0.8482				0.9043	0.7558
		0.9					0.9439					0.9439					0.9307				0.9769	0.9241

## 1339 J ADDITIONAL SYNTHETIC EXPERIMENTS RESULTS

## 1340 J.1 MAIN RESULTS SUPPLEMENT OF EXAMPLE (B) OF FIGURE 3.

1341 **Dataset Generation.** The base variables  $\{X_0, X_1, X_2, X_6, X_7\}$  are independently generated from a  
1342 Bernoulli distribution, each with  $p = 0.5$ . Subsequently, the values for  $\{X_3, X_4, X_5\}$  are determin-  
1343 istically derived using the ground truth logical rules depicted in Figure 3. Specifically, these rules  
1344 are:

$$1345 \begin{aligned} X_3 &\leftarrow X_0 \wedge X_1 \\ 1346 X_4 &\leftarrow X_2 \wedge X_7 \\ 1347 X_5 &\leftarrow (X_3 \wedge X_6) \vee (X_4 \wedge X_0) \end{aligned}$$

1350  
1351 Table 20: Impact of training sample size on the imputation accuracy of latent predicates  
1352 (`abnormal`, `fly`) in the Birds domain. Results are reported as mean  $\pm$  std over 10 random seeds,  
1353 evaluated with 10% observation probability.

# Samples	Acc. Abnormal Bird	Acc. Can Fly
100	$0.896 \pm 0.058$	$0.845 \pm 0.148$
500	$0.976 \pm 0.054$	$0.928 \pm 0.066$
1000	$0.951 \pm 0.067$	$0.928 \pm 0.066$
1500	$0.949 \pm 0.070$	$0.952 \pm 0.066$
2000	$0.951 \pm 0.067$	$0.928 \pm 0.066$

1361 Finally, to introduce missing information, a portion of the values for  $X_3$ ,  $X_4$ , and  $X_5$  are randomly  
1362 masked. These masked variables become the targets for imputation. In our experiments, we vary the  
1363 level of missingness, applying masking probabilities of 70%, 80%, and 90% to these target variables  
1364 (corresponding to observation ratios of 30%, 20%, and 10%, respectively).

1365 **Main Results.** As demonstrated in a previous case study (Table 3, which shows three runs using  
1366 the same seed but different internal rule optimization orders), variations in the rule optimization  
1367 sequence within a single seed can affect training efficiency. We thus show the coordinate descent  
1368 training progress under a different random optimization order from Figure 4 here in Figure 9. In this  
1369 run, the optimization order is  $[X_5, X_4, X_3]$  for cycle 1 and  $[X_4, X_5, X_3]$  for cycle 2. Given such  
1370 different learning trajectories, our model still discovers the correct rules successfully.

1371 Furthermore, random initialization across different seeds can lead to the discovery of varied rule  
1372 sets, and occasionally, the model might converge to a local optimum. However, as the analysis of  
1373 convergence before, performing multiple runs with different initializations enhances the probability  
1374 of identifying the global optimal solution. Our findings indicate that the model can finds global  
1375 optima several times within 20 random seeds (Tables 23 and 24).

1376 **Learning Efficiency.** As the observation ratio decreases, the guidance signal becomes less infor-  
1377 mative, reducing both rule structure recovery and missing value imputation. We also evaluated the  
1378 model’s performance with a smaller training set of 10,000 samples. The results, detailed in Tables  
1379 21 and 22, demonstrate that our model maintains high accuracy for simple AND rule learning and  
1380 predicate inference. Even for challenging OR rule learning, the model successfully identifies most  
1381 body predicates. We further investigated the impact of dataset sample size, varying it from 1,000  
1382 to 20,000 samples. As shown in Figure 8, the most efficient setting we can recover the OR rule for  
1383  $X_5$  is to use an observation ratio of 0.1 and a dataset of 4,000 samples. For the simpler AND rules  
1384 governing  $X_3$  and  $X_4$ , correct rule structures could be learned with 1,000 or even smaller samples  
1385 and a 0.1 observation ratio.

1386 Table 21: Summary of synthetic data experiment results for example (b) of the Figure 3. Each  
1387 observation ratio is evaluated using 10,000 samples and results are averaged over 20 random seeds.  
1388

Obs. Ratio	Avg. Imputation Accu. (Before Fine-tune)	Avg. Imputation Accu. (After Fine-tune)	Train Loss (Before Fine-tune)	Train Loss (After Fine-tune)
0.3	$X_3 : 0.91 \pm 0.014$	/	$X_3 : 0.069 \pm 0.007$	/
	$X_4 : 0.93 \pm 0.013$	/	$X_4 : 0.054 \pm 0.006$	/
	$X_5 : 0.87 \pm 0.003$	$X_5 : 0.88 \pm 0.002$	$X_5 : 0.110 \pm 0.002$	$X_5 : 0.103 \pm 0.000$
0.2	$X_3 : 0.91 \pm 0.014$	/	$X_3 : 0.067 \pm 0.007$	/
	$X_4 : 0.90 \pm 0.015$	/	$X_4 : 0.072 \pm 0.007$	/
	$X_5 : 0.86 \pm 0.003$	$X_5 : 0.87 \pm 0.003$	$X_5 : 0.116 \pm 0.002$	$X_5 : 0.105 \pm 0.001$
0.1	$X_3 : 0.90 \pm 0.015$	/	$X_3 : 0.075 \pm 0.007$	/
	$X_4 : 0.91 \pm 0.014$	/	$X_4 : 0.063 \pm 0.006$	/
	$X_5 : 0.85 \pm 0.003$	$X_5 : 0.88 \pm 0.002$	$X_5 : 0.124 \pm 0.002$	$X_5 : 0.107 \pm 0.001$

Table 22: Summary of learned rule structures and accuracy for example (b) of Figure 3. Each observation ratio is evaluated using 10,000 samples, with results averaged over 20 random seeds. We present the top 3 learned rule structures in order of discovery accuracy. Rule accuracy indicates the percentage of 20 runs in which a rule was learned completely correctly.

Obs. Ratio	Learned Rule Structure	Rule Accu.
0.3	$X_3 : X_0 \wedge X_1, X_0 \wedge X_6, X_1 \wedge X_7$ $X_4 : X_2 \wedge X_7, X_6 \wedge X_7, X_7$ $X_5 : (X_0 \wedge X_4) \vee (X_3 \wedge X_6), (X_3 \wedge X_4) \vee (X_3 \wedge X_6), (X_0 \wedge X_1) \vee (X_0 \wedge X_4)$	$X_3 : 0.65$ $X_4 : 0.70$ $X_5 : 0.10$
0.2	$X_3 : X_0 \wedge X_1, X_0, X_0 \wedge X_2$ $X_4 : X_2 \wedge X_7, X_2, X_6 \wedge X_7$ $X_5 : (X_0 \wedge X_4) \vee (X_3 \wedge X_6), (X_3 \wedge X_4) \vee (X_3 \wedge X_6), (X_0) \vee (X_1 \wedge X_6)$	$X_3 : 0.65$ $X_4 : 0.60$ $X_5 : 0.10$
0.1	$X_3 : X_0 \wedge X_1, X_0 \wedge X_2, X_0 \wedge X_6$ $X_4 : X_2 \wedge X_7, X_2, X_6 \wedge X_7$ $X_5 : (X_3 \wedge X_4) \vee (X_3 \wedge X_6), (X_0 \wedge X_1) \vee (X_0 \wedge X_4), (X_0 \wedge X_4) \vee (X_3 \wedge X_6)$	$X_3 : 0.60$ $X_4 : 0.65$ $X_5 : 0.10$

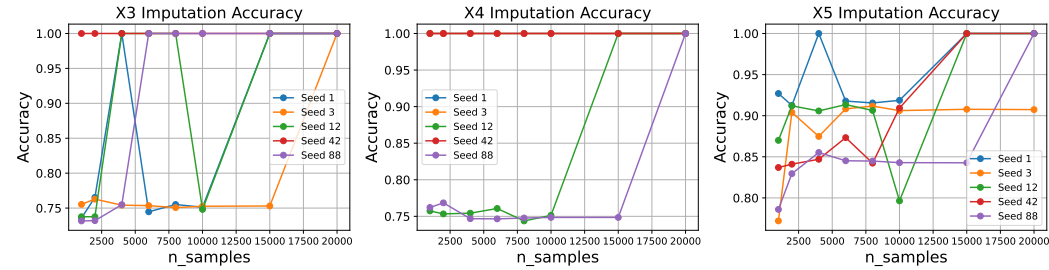


Figure 8: Imputation accuracy versus dataset sample size for Figure 3 (b). For these experiments, 10% of the data was observed (i.e., a 90% missing ratio) for predicates in  $X_3$ ,  $X_4$ , and  $X_5$ .

## J.2 RESULTS OF EXAMPLE (A) OF FIGURE 3

**Dataset Generation.** The base variables  $\{X_0, X_1, X_2, X_6\}$  are independently generated from a Bernoulli distribution, each with  $p = 0.5$ . Subsequently, the values for  $\{X_3, X_4, X_5\}$  are deterministically derived using the ground truth logical rules depicted in Figure 3. Specifically, these rules are:

$$\begin{aligned} X_3 &\leftarrow X_0 \wedge X_1 \\ X_4 &\leftarrow X_2 \wedge X_3 \\ X_5 &\leftarrow X_4 \wedge X_6 \end{aligned}$$

Finally, to introduce missing information, a portion of the values for  $X_3$ ,  $X_4$ , and  $X_5$  are randomly masked. These masked variables become the targets for imputation. In our experiments, we vary the

Table 23: Summary of synthetic data experiment results for example (b) of the Figure 3. Evaluated on 50,000 samples and results are averaged over 20 random seeds.

Obs. Ratio	Avg. Imputation Accu. (Before Fine-tune)	Avg. Imputation Accu. (After Fine-tune)	Train Loss (Before Fine-tune)	Train Loss (After Fine-tune)
0.3	$X_3 : 0.98 \pm 0.006$ $X_4 : 1.00 \pm 0.000$ $X_5 : 0.94 \pm 0.003$	$X_5 : 0.96 \pm 0.003$	$X_3 : 0.024 \pm 0.003$ $X_4 : 0.005 \pm 0.000$ $X_5 : 0.054 \pm 0.002$	$X_5 : 0.065 \pm 0.001$
0.2	$X_3 : 1.00 \pm 0.000$ $X_4 : 0.95 \pm 0.010$ $X_5 : 0.93 \pm 0.003$	$X_5 : 0.96 \pm 0.002$	$X_3 : 0.005 \pm 0.000$ $X_4 : 0.041 \pm 0.005$ $X_5 : 0.063 \pm 0.003$	$X_5 : 0.067 \pm 0.001$
0.1	$X_3 : 1.00 \pm 0.000$ $X_4 : 1.00 \pm 0.000$ $X_5 : 0.93 \pm 0.003$	$X_5 : 0.94 \pm 0.002$	$X_3 : 0.005 \pm 0.000$ $X_4 : 0.005 \pm 0.000$ $X_5 : 0.056 \pm 0.002$	$X_5 : 0.073 \pm 0.001$

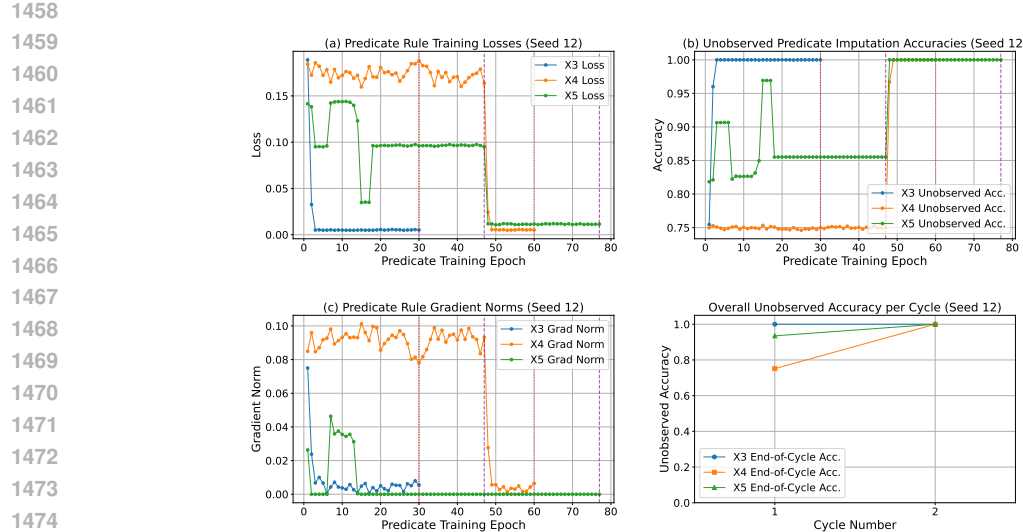


Figure 9: Training dynamics for a representative run (Obs. Ratio = 0.3) of Figure 3 (b). The optimization order:  $[X_5, X_4, X_3]$  for Cycle 1;  $[X_4, X_5, X_3]$  for Cycle 2. Subplots display: (a) training losses, (b) unobserved imputation accuracies, and (c) gradient norms for rule embeddings; (d) overall imputation accuracies each cycle. Red dashed lines indicate the conclusion of training blocks for  $X_3$  or  $X_4$  (each allocated 30 epochs when active within a cycle). Purple dashed lines delineate training phases for  $X_5$  (Rule 1, Rule 2, and Fine-tune); the epoch count for these  $X_5$  phases can vary per cycle due to the dynamic nature of the hard covering mechanism. Correct rule structures were learned for  $X_3$  by the end of Cycle 1, and for  $X_4$  and  $X_5$  by the end of Cycle 2.

Table 24: Summary of learned rule structures and accuracy for example (b) of Figure 3. Each observation ratio was evaluated using 50,000 samples, with results averaged over 20 random seeds. We present the top 3 learned rule structures in order of discovery accuracy. Rule accuracy indicates the percentage of 20 runs in which a rule was learned completely correctly.

Obs. Ratio	Learned Rule Structure	Rule Accu.
0.3	$X_3 : X_0 \wedge X_1, X_0 \wedge X_2$ $X_4 : X_2 \wedge X_7$ $X_5 : (X_0 \wedge X_4) \vee (X_3 \wedge X_6), (X_3 \wedge X_4) \vee (X_3 \wedge X_6), (X_0 \wedge X_4) \vee (X_1 \wedge X_3)$	$X_3 : 0.90$ $X_4 : 1.00$ $X_5 : 0.50$
0.2	$X_3 : X_0 \wedge X_1$ $X_4 : X_2 \wedge X_7, X_0 \wedge X_7, X_2$ $X_5 : (X_0 \wedge X_4) \vee (X_3 \wedge X_6), (X_3 \wedge X_4) \vee (X_3 \wedge X_6), (X_0 \wedge X_1) \vee (X_0 \wedge X_4)$	$X_3 : 1.00$ $X_4 : 0.80$ $X_5 : 0.40$
0.1	$X_3 : X_0 \wedge X_1$ $X_4 : X_2 \wedge X_7$ $X_5 : (X_0 \wedge X_4) \vee (X_3 \wedge X_6), (X_3 \wedge X_4) \vee (X_3 \wedge X_6), (X_0 \wedge X_1) \vee (X_0 \wedge X_4)$	$X_3 : 1.00$ $X_4 : 1.00$ $X_5 : 0.30$

level of missingness, applying masking probabilities of 70%, 80%, and 90% to these target variables (corresponding to observation ratios of 30%, 20%, and 10%, respectively).

**Main Results.** We show the coordinate descent training progress under different random optimization order. Figure 10 demonstrates the convergence in two cycles, while Figure 11 requires three cycles to complete training.

We summarize the results for example (a) of the Figure 3 in Tables 25 and 26, which demonstrate both the effectiveness of our rule discovery approach and the precision of missing variables imputation. Our analysis reveals that learning the multi-step chain structure presents significant challenges, primarily because the algorithm uses inferred predicate values  $v^t$  from previous steps to update the current values by Eq. 3. This creates a dependency chain where suboptimal rule embeddings learned at earlier optimization steps can propagate errors to subsequent steps, potentially degrading overall performance. Despite these challenges, our model successfully identifies the correct rules in the majority of experimental runs. This robustness indicates that with multiple random initializations, the

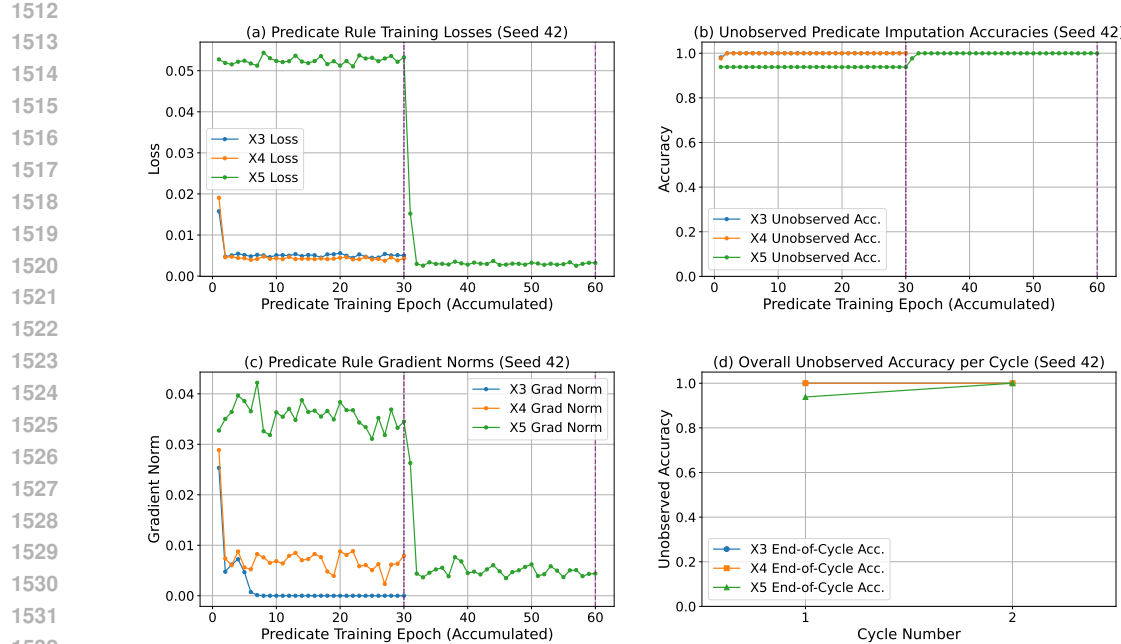


Figure 10: Training dynamics for a representative run (Observation Ratio = 0.2) of Figure 3 (a). Subplots display: (a) training losses, (b) unobserved imputation accuracies, and (c) gradient norms for rule embeddings; (d) overall imputation accuracies each cycle. Purple dashed lines indicate the conclusion of training blocks for one cycle (each allocated 30 epochs). The rule embedding optimization order: [  $X_5, X_3, X_4$  ] for Cycle 1; [  $X_5, X_4, X_3$  ] for Cycle 2. Correct rule structures were learned for  $X_3$  and  $X_4$  by the end of Cycle 1, for  $X_5$  by the end of Cycle 2. The learned rules:  $X_3 \leftarrow X_0 \wedge X_1, X_4 \leftarrow X_2 \wedge X_3, X_5 \leftarrow X_4 \wedge X_6$ .

algorithm reliably converges to the optimal rule structures like the results from Figures 10 and 11, which effectively overcome the inherent difficulties of sequential dependency learning in chain-like logical structures.

Table 25: Summary of synthetic data experiment results for example (a) of the Figure 3. Each observation ratio is evaluated using 50,000 samples and results are averaged over 20 random seeds. No fine-tune phase since we assume no disjunctive rules.

Obs. Ratio	Avg. Imputation Accu.	Train Loss
0.3	$X_3 : 0.86 \pm 0.13$	$X_3 : 0.09 \pm 0.08$
	$X_4 : 0.91 \pm 0.06$	$X_4 : 0.07 \pm 0.04$
	$X_5 : 0.95 \pm 0.03$	$X_5 : 0.04 \pm 0.02$
0.2	$X_3 : 0.85 \pm 0.13$	$X_3 : 0.10 \pm 0.08$
	$X_4 : 0.90 \pm 0.05$	$X_4 : 0.08 \pm 0.04$
	$X_5 : 0.94 \pm 0.02$	$X_5 : 0.04 \pm 0.02$
0.1	$X_3 : 0.82 \pm 0.12$	$X_3 : 0.10 \pm 0.07$
	$X_4 : 0.90 \pm 0.05$	$X_4 : 0.08 \pm 0.04$
	$X_5 : 0.94 \pm 0.02$	$X_5 : 0.05 \pm 0.02$

### J.3 RESULTS OF EXAMPLE (C) OF FIGURE 3

**Dataset Generation.** The base variables  $\{X_0, X_1, X_2, X_6, X_7\}$  are independently generated from a Bernoulli distribution, each with  $p = 0.5$ . Subsequently, the values for  $\{X_3, X_4, X_5, X_8\}$  are deterministically derived using the ground truth logical rules depicted in Figure 3. Specifically,

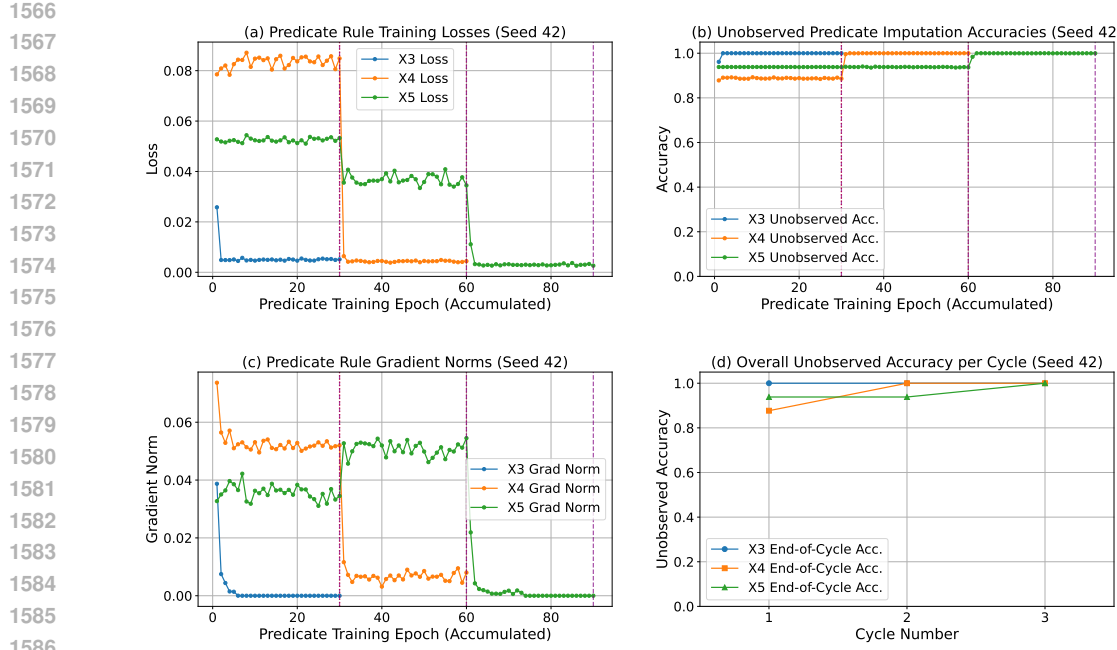


Figure 11: Training dynamics for a representative run (Observation Ratio = 0.2) of Figure 3 (a). Subplots display: (a) training losses, (b) unobserved imputation accuracies, and (c) gradient norms for rule embeddings; (d) overall imputation accuracies each cycle. Purple dashed lines indicate the conclusion of training blocks for one cycle (each allocated 30 epochs). The rule embedding optimization order:  $[X_5, X_4, X_3]$  for Cycle 1,2;  $[X_3, X_5, X_4]$  for Cycle 3. Correct rule structures were learned for  $X_3$  by the end of Cycle 1, for  $X_4$  by the end of Cycle 2, and for  $X_5$  by the end of Cycle 3. The learned rules:  $X_3 \leftarrow X_0 \wedge X_1$ ,  $X_4 \leftarrow X_2 \wedge X_3$ ,  $X_5 \leftarrow X_4 \wedge X_6$ .

Table 26: Summary of learned rule structures and accuracy for example (a) of Figure 3. Each observation ratio is evaluated using 50,000 samples, with results averaged over 20 random seeds. We present the top 3 learned rule structures in order of discovery accuracy. The rules that are truth rules are indicated by underline. Rule accuracy indicates the percentage of 20 runs in which a rule was learned completely correctly.

Obs. Ratio	Learned Rule Structure	Rule Accuracy
0.3	$X_3 : X_0 \wedge X_1, X_0 \wedge X_4, X_5$ $X_4 : X_2 \wedge X_3, \underline{X_3} \wedge X_5, X_0 \wedge X_5$ $X_5 : \underline{X_4} \wedge X_6, X_3 \wedge X_4, X_1 \wedge X_4$	$X_3 : 0.60$ $X_4 : 0.40$ $X_5 : 0.40$
0.2	$X_3 : X_0 \wedge X_1, X_5, X_0 \wedge X_5$ $X_4 : X_2 \wedge X_3, X_5 \wedge X_3, X_5$ $X_5 : \underline{X_4} \wedge X_6, X_4, X_3 \wedge X_4$	$X_3 : 0.40$ $X_4 : 0.30$ $X_5 : 0.20$
0.1	$X_3 : X_0 \wedge X_1, X_0 \wedge X_4, X_0 \wedge X_5$ $X_4 : X_2 \wedge X_3, X_5, X_2 \wedge X_5$ $X_5 : \underline{X_4} \wedge X_6, X_4 \wedge X_2, X_3 \wedge X_6$	$X_3 : 0.40$ $X_4 : 0.40$ $X_5 : 0.10$

these rules are:

$$\begin{aligned}
 X_3 &\leftarrow X_0 \wedge X_1 \\
 X_4 &\leftarrow X_2 \wedge X_7 \\
 X_8 &\leftarrow X_4 \wedge X_0 \\
 X_5 &\leftarrow (X_3 \wedge X_6) \vee (X_8) \vee (X_6 \wedge X_7)
 \end{aligned}$$

Finally, to introduce missing information, a portion of the values for  $X_3, X_4, X_8$  and  $X_5$  are randomly masked. These masked variables become the targets for imputation. In our experiments, we

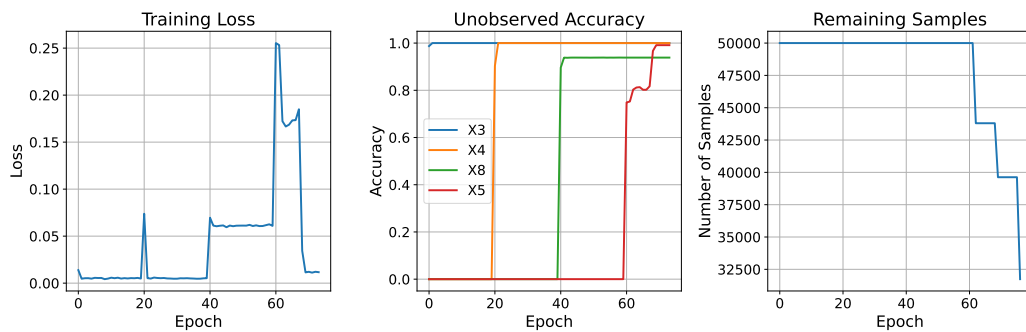
1620 vary the level of missingness, applying masking probabilities of 70%, 80%, and 90% to these target  
 1621 variables (corresponding to observation ratios of 30%, 20%, and 10%, respectively).

1622 **Main Results.** We summarize the results for example (c) of the Figure 3 in the Tables 27 and 28,  
 1623 showcasing the effectiveness of rule discovery and the precision of missing variables imputation.  
 1624 We have random coordinate descent training order for rule optimization.

1625 This task is more challenging due to the chain-like structure of the disjunctive rules, particularly  
 1626 with three clauses for  $X_5$ , resulting in lower learning accuracy than in example (b). Nonetheless, our  
 1627 method achieves the highest rule discovery accuracy for the ground-truth rules while maintaining  
 1628 acceptable imputation accuracy. For the most difficult prediction task ( $X_5$ ), we obtain over 80%  
 1629 accuracy across all three observation ratios. Other predicate predictions reach  $\sim 90\%$  accuracy,  
 1630 including the chain-derived predicate  $X_8$ . For the learned rules in Table 28, we can find most body  
 1631 predicates are correct even for the complex three-clause rules governing  $X_5$ , which include the  
 1632 chain-derived predicate  $X_8$ . We also show the loss plot for one run in Figure 12.

1633 Table 27: Summary of synthetic data experiment results for example (c) of the Figure 3. Each  
 1634 observation ratio is evaluated using 50,000 samples and results are averaged over 20 random seeds.  
 1635

Obs. Ratio	Avg. Imputation Accu. (Before Fine-tune)	Avg. Imputation Accu. (After Fine-tune)	Train Loss (Before Fine-tune)	Train Loss (After Fine-tune)
0.3	$X_3 : 0.86 \pm 0.12$	/	$X_3 : 0.102 \pm 0.09$	/
	$X_4 : 0.87 \pm 0.13$	/	$X_4 : 0.093 \pm 0.09$	/
	$X_5 : 0.79 \pm 0.09$	$X_5 : 0.84 \pm 0.08$	$X_5 : 0.111 \pm 0.06$	$X_5 : 0.147 \pm 0.08$
	$X_8 : 0.91 \pm 0.06$	/	$X_8 : 0.060 \pm 0.04$	/
0.2	$X_3 : 0.89 \pm 0.12$	/	$X_3 : 0.083 \pm 0.09$	/
	$X_4 : 0.88 \pm 0.12$	/	$X_4 : 0.087 \pm 0.08$	/
	$X_5 : 0.78 \pm 0.08$	$X_5 : 0.82 \pm 0.09$	$X_5 : 0.119 \pm 0.06$	$X_5 : 0.159 \pm 0.08$
	$X_8 : 0.93 \pm 0.06$	/	$X_8 : 0.046 \pm 0.04$	/
0.1	$X_3 : 0.89 \pm 0.12$	/	$X_3 : 0.084 \pm 0.09$	/
	$X_4 : 0.89 \pm 0.12$	/	$X_4 : 0.084 \pm 0.09$	/
	$X_5 : 0.78 \pm 0.10$	$X_5 : 0.80 \pm 0.11$	$X_5 : 0.133 \pm 0.07$	$X_5 : 0.169 \pm 0.10$
	$X_8 : 0.93 \pm 0.06$	/	$X_8 : 0.048 \pm 0.04$	/



1664 Figure 12: An example of loss and imputation accuracy during coordinate optimization (Obs. Ratio  
 1665 = 0.1, seed = 88, from example (c) of Figure 3). The training order is  $[X_3, X_4, X_8, X_5]$ . Epochs 0–19  
 1666 correspond to rule learning for  $X_3$ ; epochs 20–39 for  $X_4$ ; epochs 40–59 for  $X_8$ , and epochs 60–end  
 1667 for  $X_5$ . Remaining samples identified how many samples are “well-explained” during hard covering  
 1668 phase. As the imputation accuracy for missing  $X_5$  is 1.00, we do not go to the fine-tune phase. The  
 1669 learned rules:  $X_3 \leftarrow X_0 \wedge X_1, X_4 \leftarrow X_2 \wedge X_7, X_5 \leftarrow (X_3 \wedge X_6) \vee X_8 \vee (X_6 \wedge X_7), X_8 \leftarrow X_3 \wedge X_4$ .  
 1670

#### 1671 J.4 HYPER-PARAMETERS SETTING AND COMPUTING RESOURCE

1672 Our model operates efficiently in a CPU environment utilizing the PyTorch library. The hyperpa-  
 1673 rameters are configured as follows:

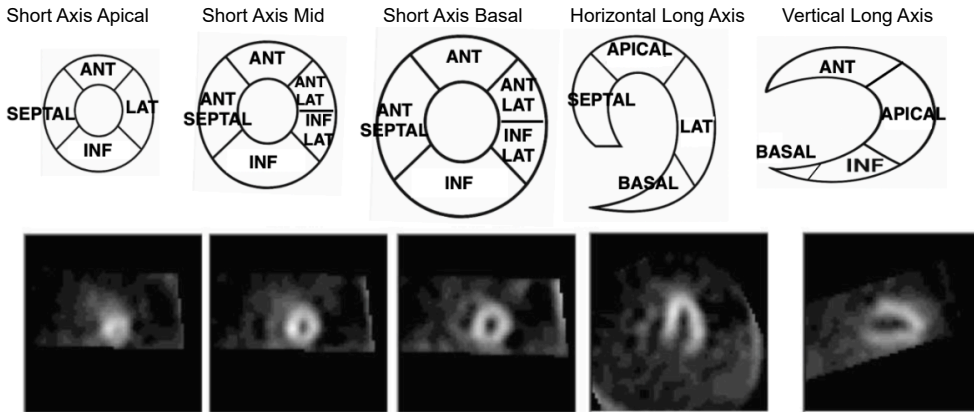
1674  
 1675 Table 28: Summary of learned rule structures and accuracy for example (c) of Figure 3. Each  
 1676 observation ratio is evaluated using 50,000 samples, with results averaged over 20 random seeds.  
 1677 We present the top 3 learned rule structures in order of discovery accuracy. The rules that are truth  
 1678 rules are indicated by underline. Rule accuracy indicates the percentage of 20 runs in which a rule  
 1679 was learned completely correctly.

1680	Obs. Ratio	Learned Rule Structure	Rule Accu.
1681	0.3	$X_3 : X_0 \wedge X_1, X_0 \wedge X_2, X_1 \wedge X_2$ $X_4 : \underline{X_2 \wedge X_7}, X_1 \wedge X_2, X_2$ $X_5 : \underline{(X_3 \wedge X_6) \vee X_8 \vee (X_6 \wedge X_7)}, X_4 \vee (X_3 \wedge X_6) \vee (X_6 \wedge X_7),$ $(X_3 \wedge X_4) \vee X_3 \vee (X_3 \wedge X_7)$ $X_8 : \underline{X_4 \wedge X_0}, X_3 \wedge X_7, X_2 \wedge X_0$	$X_3 : 0.45$ $X_4 : 0.5$ $X_5 : 0.15$ $X_8 : 0.3$
1682			
1683			
1684			
1685			
1686	0.2	$X_3 : X_0 \wedge X_1, X_1 \wedge X_2, X_0 \wedge X_2$ $X_4 : \underline{X_2 \wedge X_7}, X_0 \wedge X_2, X_1 \wedge X_2$ $X_5 : \underline{(X_3 \wedge X_6) \vee X_8 \vee (X_6 \wedge X_7)}, (X_2 \wedge X_3) \vee X_4 \vee (X_6 \wedge X_7),$ $X_8 : \underline{X_4 \wedge X_0}, X_3 \wedge X_4, X_3 \wedge X_7$	$X_3 : 0.55$ $X_4 : 0.55$ $X_5 : 0.10$ $X_8 : 0.25$
1687			
1688			
1689			
1690			
1691	0.1	$X_3 : \underline{X_0 \wedge X_1}, X_0, X_0 \wedge X_7$ $X_4 : \underline{X_2 \wedge X_7}, \underline{X_0 \wedge X_2}, X_1 \wedge X_7$ $X_5 : X_4 \vee X_8 \vee (X_6 \wedge X_7), \underline{(X_3 \wedge X_6) \vee X_8 \vee (X_6 \wedge X_7)},$ $X_8 : \underline{X_4 \wedge X_0}, X_2 \wedge X_4, X_3 \wedge X_7$	$X_3 : 0.55$ $X_4 : 0.55$ $X_5 : 0.10$ $X_8 : 0.2$
1692			
1693			
1694			
1695			

1696  
 1697 • Rule Embedding and Fine-tuning Optimizer: Adam, learning rate: 0.01.  
 1698 • Temperature of softmin and softmax: 0.1 (for Eq. 4) and 10.0 for (Eq. 5).  
 1699 • “Well-explained” Threshold: 0.99 (for sequential hard covering in disjunctive rule learning).  
 1700 • Batch Size: 64 .

## 1702 K ADDITIONAL REAL WORLD DATA EXPERIMENTS RESULTS

### 1703 K.1 SPECT



1721 Figure 13: The five slices consists of 22 regions of interest (ROI) for SPECT Diagnosis. The slices  
 1722 are chosen according to the following: Three slices for short axis view-one slice near heart’s apex,  
 1723 one in middle of the LV and one near the heart base; One slice corresponds to the center of the LV  
 1724 cavity for horizontal long axis view; One slice corresponds to the center of the LV cavity for vertical  
 1725 long axis view (Kurgan et al., 2001).

1726 We ask for an expertise from cardiovascular surgery of a hospital to give us domain knowledge, and  
 1727 then we try to explain the learned rules. We select several meaningful rules to demonstrate.

The domain knowledge are as follows.

- R1: The anterior wall and the septum of the left ventricle are adjacent and often simultaneously affected by the Left Anterior Descending artery (LAD). If both anterior wall and septum show infarction, it strongly suggests an issue with the LAD. If both apical anterior and mid-anterior show infarction, it indicates a more extensive problem within the LAD territory, affecting both the apical and mid-portions of the anterior wall.
- R2: The apical lateral wall (typically LCX territory) and the apical inferior wall (typically RCA or LCX territory) are adjacent. Infarction in both suggests a problem in this combined region.
- R3: If both apical septal and apical septal show infarction, it indicates a more extensive problem in the LAD territory, involving ischemia in multiple myocardial segments.
- R4: If apical lateral and apical lateral show infarction, it indicates a more extensive ischemic problem in the Left Circumflex artery (LCX) territory.
- R5: The apical anterior (ANT) and apical septal (SEPTAL) regions are primarily supplied by the Left Anterior Descending artery (LAD); the apical lateral (LAT) region is primarily supplied by the Left Circumflex artery (LCX); the apical inferior (INF) region is primarily supplied by the Right Coronary Artery (RCA), but can sometimes be supplied by the LCX, depending on the coronary artery dominance pattern.

Refer to Figure 13, we can give some explanations of rules learned in Table 29 based on the domain knowledge R1 to R5. For example,

- $F_5 \leftarrow F_1 \wedge F_2$ :  $F_1$  and  $F_2$  are features from the first slice near the heart’s apex, while  $F_5$  is from the second slice at the middle of the left ventricle (LV). According to clinical knowledge R1 and R5, the anterior and septal regions are primarily supplied by the Left Anterior Descending (LAD) artery. Therefore, this rule is clinically plausible: if partial diagnosis (labeled as 1) is present in both  $F_1$  and  $F_2$ , it strongly suggests an LAD artery problem. Since  $F_5$  is in the mid-anterior region, also supplied by the LAD, it has a high probability of being affected as well.
- $Diagnosis \leftarrow F_5 \wedge F_6$ : From R1, we know that the anterior wall and the septum of the left ventricle are adjacent.  $F_5$  and  $F_6$  both from middle of the LV (left ventricular), and they are adjacent. Thus, if both these adjacent mid-ventricular regions ( $F_5$  and  $F_6$ ) show signs of infarction, it significantly increases the likelihood of an overall positive diagnosis.

Table 29: Example rules learned by NS-FCN for SPECT feature imputation and diagnosis.

#### Selected Feature Imputation Rules Learned by NS-FCN

$F_5 \leftarrow F_1 \wedge F_2$ : partial diagnosis of segment 1 and 2 causes the partial diagnosis of segment 5.  
 $F_6 \leftarrow F_{11} \wedge F_{19}$   
 $F_{13} \leftarrow F_{22} \wedge F_{12}$

#### Learned Diagnosis Rule Structure

$Diagnosis \leftarrow (F_5 \wedge F_6) \vee (F_2 \wedge F_{11}) \vee (F_4 \wedge F_{13})$

As detailed in Table 30, the learned rules for diagnosing cardiac abnormalities correspond closely with established domain knowledge from cardiovascular surgery experts. For instance, the model identified that infarcts in adjacent regions like  $F_1$  and  $F_2$  are indicative of an issue in the Left Anterior Descending (LAD) artery territory. Furthermore, the model learned a composite rule for the final diagnosis, logically aggregating signals from multiple infarcted regions across different coronary artery territories (LAD, LCX, RCA). This ability to synthesize information from disparate features into a coherent diagnostic rule highlights the model’s capacity for complex reasoning. The clinical relevance of these rules was further validated by a Large Language Model (LLM), which confirmed their consistency with expert knowledge on ischemia propagation patterns.

**Performance with varying missing ratios.** To assess the model’s robustness under different levels of data scarcity, we evaluated its performance on the SPECT dataset while varying the observation ratio from 0.3 to 0.9. As shown in Table 18, the model’s accuracy remains strong and improves consistently as more data becomes available. Notably, even with only 30% of the data observed (a 70% missing ratio), the model maintains a high F1 score of 0.751, demonstrating its capability to learn meaningful diagnostic rules from highly incomplete datasets.

1782 Table 30: Analysis of learned rules for the SPECT dataset, evaluated by human experts and LLM.  
1783

1784 <b>Rules</b>	1785 <b>Evaluation with Human Expert</b>	1786 <b>LLM Evaluation</b>
1787 $F_6 \leftarrow F_1 \wedge F_2$	1788 Matches R1 & R5: $F_1$ and $F_2$ are in LAD territory. Infarction in both suggests LAD issue affecting apical and mid-anterior LV.	1789 <b>Plausible:</b> Both regions are LAD-supplied and adjacent; mid-anterior ( $F_3$ ) likely also affected if $F_1$ & $F_2$ show infarction. Clinically consistent.
1790 $F_0 \leftarrow F_{11} \wedge F_{19}$	1791 Related to R2 & R4: $F_{11}$ and $F_{19}$ are adjacent. Infarction implies LCX or RCA/LCX combined territory issue.	1792 <b>Valid:</b> Matches adjacency and vascular territory logic (LCX-lateral, RCA-inferior). Supports ischemia propagation in midventricular slices.
1793 $F_{13} \leftarrow F_{22} \wedge F_{12}$	1794 Partial link to R3 & R5: Likely involves basal/apical septal ( $F_{22}$ ) and adjacent basal regions. Indicates LAD or multi-segment ischemia.	1795 <b>Reasonable:</b> Suggests ischemia spread in basal-septal regions (LAD) adjacent to basal/anterior. Fits multi-segment LAD pathology.
1796 $\text{Diagnosis} \leftarrow (F_1 \wedge F_0) \vee (F_2 \wedge F_{11}) \vee (F_6 \wedge F_{13})$	1797 Diagnosis $\leftarrow (F_1 \wedge F_0) \vee (F_2 \wedge F_{11}) \vee (F_6 \wedge F_{13})$ Consistent with R1 & R4. Combines LAD ( $F_0$ ), LCX/RCA ( $F_6$ ), and adjacent mixed regions. Multiple adjacent infarct pairs increase diagnosis likelihood.	1798 <b>Strong:</b> Logical aggregation of adjacent infarcted regions across LAD, LCX, RCA territories. Matches expert ischemia propagation patterns.

1803 

## K.2 HEART DISEASE

1804 

### K.2.1 ASSESSMENT OF LEARNED RULES

1805 For feature imputation, as shown in Table 31, our model discovers rules with clinically relevant  
1806 numerical thresholds by directly modeling continuous data. For instance, it learns to impute resting  
1807 blood pressure (`trestbps`) based on conditions like `age > 60` and `chol > 250`. Similarly, it links  
1808 high cholesterol to factors like `age > 55` in males or very high blood pressure (`trestbps > 150`). The  
1809 learned rule for ST depression (`oldpeak`) combines the slope of the ST segment with a maximum  
1810 heart rate threshold (`thalach < 150`), demonstrating the model’s ability to capture complex, non-  
1811 linear relationships within the data.

1812 Beyond imputation, NS-FCN learns interpretable rules for the final diagnosis, classifying patients  
1813 into low-risk or high-risk categories.

1814 Table 32 presents several of these diagnostic rules. For example, the model learns that a  
1815 combination of factors such as an upsloping ST segment (`slope_upsloping`), a fixed thallium defect  
1816 (`thal_fixed_defect`), and exercise-induced angina (`exang_yes`) is strongly indicative of high risk. Con-  
1817 versely, it identifies that factors like the absence of exercise-induced angina (`exang_no`) and a flat  
1818 ST slope (`slope_flat`) in female patients suggest a low risk of coronary artery disease. These diag-  
1819 nóstic rules were also evaluated by an LLM and deemed “Excellent” or “Strong,” underscoring their  
1820 consistency with clinical practice.

1821 

## K.3 HYPER-PARAMETERS SETTING AND COMPUTING RESOURCE

1822 For NS-FCN (Ours):

- 1823 • Rule embedding optimizer: Adam with learning rate of 0.01.
- 1824 • Fine-tune optimizer: Adam with learning rate of 0.01.
- 1825 • **Temperature of softmin and softmax: 0.1 (for Eq. 4) and 10.0 for (Eq. 5).**
- 1826 • Our model can run efficiently on a CPU environment with the PyTorch package.

1827 **Baselines:**

- 1828 • **BRCG** (Dash et al., 2018), **LEN** (Barbiero et al., 2022), **DR-NET** (Qiao et al., 2021),  
1829 **RRL** (Wang et al., 2021) are trained with the default hyperparameter settings specified in  
1830 the original paper.
- 1831 • **MICE** (van Buuren & Groothuis-Oudshoorn, 2011): We use  $m = 5$  imputations and  
1832  $maxit = 5$  iterations with the default imputation methods in the `mice` R package.

1836 Table 31: Learned rules for feature imputation on the Heart dataset, with LLM assessments.  
1837

1838 <b>Feature</b>	1839 <b>Imputation Acc.</b>	1840 <b>Learned Rule</b>	1841 <b>LLM Assessment</b>
1840 trestbps	1841 0.86	1842 $trestbps\_high \leftarrow (age > 60) \wedge (chol > 250)$	1843 <b>Excellent:</b> This rule captures the well-established link between age, high cholesterol, and hypertension. Both are primary risk factors for cardiovascular disease and often co-occur.
1844 chol	1845 0.85	1846 $chol\_high \leftarrow (sex = 1 \wedge age > 55) \vee (trestbps > 150)$	1847 <b>Excellent:</b> The rule correctly identifies 1848 two key risk profiles for high cholesterol: 1849 middle-aged to elderly males, and individuals 1850 with significant hypertension. This 1851 aligns perfectly with clinical understanding 1852 of metabolic syndrome.
1850 thalach	1851 0.90	1852 $hr\_high \leftarrow (trestbps > 145) \vee (age > 57 \wedge cp = 3)$	1853 <b>Strong:</b> This rule insightfully links 1854 factors that limit exercise capacity to the 1855 maximum heart rate achieved. Both 1856 hypertension and severe asymptomatic coronary 1857 disease can prevent a patient from reaching 1858 a higher peak heart rate.
1859 oldpeak	1860 0.76	1861 $st\_severe \leftarrow (slope = 2) \wedge (thalach < 150)$	1862 <b>Excellent:</b> This rule identifies a classic 1863 high-risk pattern. A downsloping ST segment 1864 is a strong positive finding, and its occurrence 1865 at a sub-maximal heart rate indicates 1866 ischemia at a low workload, a sign of 1867 severe coronary artery disease.

1862 Table 32: Learned rules for disease prediction on the Heart dataset, with LLM assessments.  
1863

1864 <b>Learned Rule</b>	1865 <b>LLM Assessment</b>
1866 $high\_risk \leftarrow restecg\_stt\_abnormality \wedge ca = 3 \wedge oldpeak > 1.49$	1867 <b>Excellent:</b> This rule identifies a high-risk profile by 1868 combining three critical indicators of severe coronary artery 1869 disease: significant ST depression, an abnormal resting ECG, and extensive vessel blockage.
1870 $high\_risk \leftarrow slope\_downsloping \wedge restecg\_normal \wedge trestbps > 145.68$	1871 <b>Strong:</b> A downsloping ST segment is a powerful predictor 1872 of ischemia. Combining this with hypertension identifies 1873 patients at high risk, even if their resting ECG appears 1874 normal, highlighting the importance of stress-test indicators.
1875 $high\_risk \leftarrow slope\_flat \wedge oldpeak > 1.49 \wedge restecg\_hypertrophy$	1876 <b>Excellent:</b> This rule effectively combines signs of acute 1877 ischemia (a flat ST slope with significant depression) with 1878 evidence of chronic cardiac stress (left ventricular hypertrophy). 1879 This profile is strongly indicative of advanced coronary artery disease.

- 1880 • **MissForest** (Stekhoven & Bühlmann, 2012): We use the default hyperparameter settings  
1881 in the `missForest` R package.
- 1882 • **MLP**: We train a 3-layer fully connected network (input-128-128-output) with batch size  
1883 32, learning rate 0.001, and 100 epochs using Adam optimizer.
- 1884 • **VAE**(Veldkamp et al., 2025): We use a variational autoencoder with latent dimension 16,  
1885 encoder architecture (input $\times$ 2-128-64-latent), decoder architecture (latent-64-128-output),  
1886 batch size 32, learning rate 0.001, and 100 epochs.
- 1887 • **DAE (mDAE)** (Dupuy et al., 2024): We use a denoising autoencoder with bottleneck  
1888 dimension 16, encoder architecture (input-128-64-bottleneck), decoder architecture

1890 (bottleneck-64-128-output), corruption rate  $\rho = 0.2$ , batch size 32, learning rate 0.001, and  
 1891 100 epochs.

1892 • **GAIN** (Yoon et al., 2018): We use mini-batch size 128, hint rate  $p_{hint} = 0.9$ , MSE loss  
 1893 weight  $\alpha = 100.0$ , cross-entropy loss weight  $\beta = 100.0$ , learning rate 0.001, and 1000  
 1894 epochs.

1895 • **MissDiff** (Ouyang et al., 2023): We use 1000 diffusion timesteps with  $\beta_{start} = 10^{-4}$  and  
 1896  $\beta_{end} = 0.02$ , batch size 32, learning rate 0.001, and 100 epochs.

1897 • All baseline models can run efficiently on CPU environment with PyTorch package (for  
 1898 deep learning methods) or R packages (for statistical methods).

1899

## 1900 L LIMITATION

1901 While our model shows promising performance, the ethical implications, such as potential over-  
 1902 reliance or misuse for inferring sensitive information, require careful consideration.

1903 Despite its strengths, NS-FCN has limitations. While effective, the asynchronous coordinate  
 1904 gradient descent optimization can be computationally intensive. Besides, the negative predicates are  
 1905 not well explored (we consider negative predicates as an independent predicate from positive pred-  
 1906 icates). Furthermore, while our model can derive predicates from continuous features, the current  
 1907 implementation learns a single threshold per feature, which may not capture more complex relation-  
 1908 ships (e.g., intervals). Extending the framework to learn more expressive predicates from continuous  
 1909 data is a promising direction for future work.

## 1910 M USE OF LLMs

1911 In this paper, LLMs were used solely for writing polishing. The key idea, the model design, research  
 1912 study, and all substantive writing are completed by human authors.

1913 In the assessment of discovered rules, we use LLM to write the evaluation of rule quality, which we  
 1914 have mentioned in the paper.

1916  
 1917  
 1918  
 1919  
 1920  
 1921  
 1922  
 1923  
 1924  
 1925  
 1926  
 1927  
 1928  
 1929  
 1930  
 1931  
 1932  
 1933  
 1934  
 1935  
 1936  
 1937  
 1938  
 1939  
 1940  
 1941  
 1942  
 1943